ELSEVIER

Journal of Structural Geology 29 (2007) 298–317

JOURNAL OF STRUCTURAL GEOLOGY

www.elsevier.com/locate/jsg

Fabric attractors in general triclinic flow systems and their application to high strain shear zones: A dynamical system approach

D. Iacopini [a,*], C.W. Passchier [b], D. Koehn [b], R. Carosi [a]

[a] *Dipartimento di Scienze della Terra, Universita' degli studi di Pisa, Via S. Maria 53, 56126 Pisa, Italy*
[b] *Institut für Geowissenschaften, Tektonophysik, Universität Mainz, Germany*

Received 14 December 2005; received in revised form 25 September 2006; accepted 5 October 2006
Available online 14 December 2006

Abstract

High strain zones may deform by flow with a triclinic symmetry. This paper describes triclinic flow in a reference frame where Instantaneous Stretching Axes (ISA) are fixed. The operation of triclinic flow is described in two ways: first in terms of flow and the nature of flow eigenvectors and in the second part of the paper in terms of finite strain. In monoclinic flow, at least one of the eigenvectors of the flow coincides with one of the ISA and one or two of the eigenvectors act as attractors of foliation or lineation elements. In triclinic flow some flow eigenvectors are undefined since the two largest eigenvalues (controlling the flow) are imaginary. Imaginary eigenvalues are particularly common at high kinematic vorticity and within flow with deviation of the vorticity vector of more than 20° from one of the ISA. Strong deviation from monoclinic flow is therefore possible, but this will not produce permanent foliations or lineations. For triclinic flow that does produce permanent fabrics, the angle between ISA and the fabric is so small that it is unlikely that it can be recognised in nature. A discussion of the potential application of such results within real shear zones is presented.

Keywords: Flow kinematics; Deformation; Shear zones; Eigenvector; Ghostvector

1. Introduction

1.1. Fabric attractors in shear zones

In the last 20 years much work has focussed on understanding the influence of flow geometry on the final distribution of fabrics in deformed rocks. Several previous studies were based on steady state deformation (Ramsay and Graham, 1970; Means et al., 1980; Ramberg, 1974; Bobyarchick, 1986; Jiang and Williams, 1998; Passchier, 1997, 1998) and described the effect of flow parameters such as vorticity and volume change on the deformation geometry. Theoretical considerations show that in a homogeneous steady state progressive deformation, stable axes exist, controlled by the eigenvectors of the flow system that can behave as sinks or blocked positions for material lines and rigid objects (Fig. 1a; Ramberg, 1974; Passchier, 1986; Fossen and Tikoff, 1993). Flow eigenvectors are axes along which the angular velocity of material lines is zero in a reference frame of Instantaneous Stretching Axes (ISA), the orthogonal directions of maximum, minimum and intermediate stretching rate (Passchier, 1997). ISA are useful reference axes since they are orthogonal in any flow type. A maximum number of three eigenvectors can exist in any flow type, and these rule the motion of material lines in the flow. Eigenvectors can be three different types of axes: they can be directions towards which the material points and lines tend to migrate and where they accumulate (attractor: e in Fig. 1a); from which they tend to move away (repulsor: f in Fig. 1a) or which act as ''saddle'' directions where material lines can move towards the eigenvector in some orientations and away from it in others. All material lines close to an attractor or repulsor move permanently away or towards this axis, but for a saddle direction, only the line parallel to the axis is irrotational; all other lines pass close to the saddle

* Corresponding author. Tel.: +39 0502 215846; fax: +39 0502 215800.
E-mail address: iacopini@dst.unipi.it (D. Iacopini).

0191-8141/$ - see front matter © 2006 Elsevier Ltd. All rights reserved.
doi:10.1016/j.jsg.2006.10.002

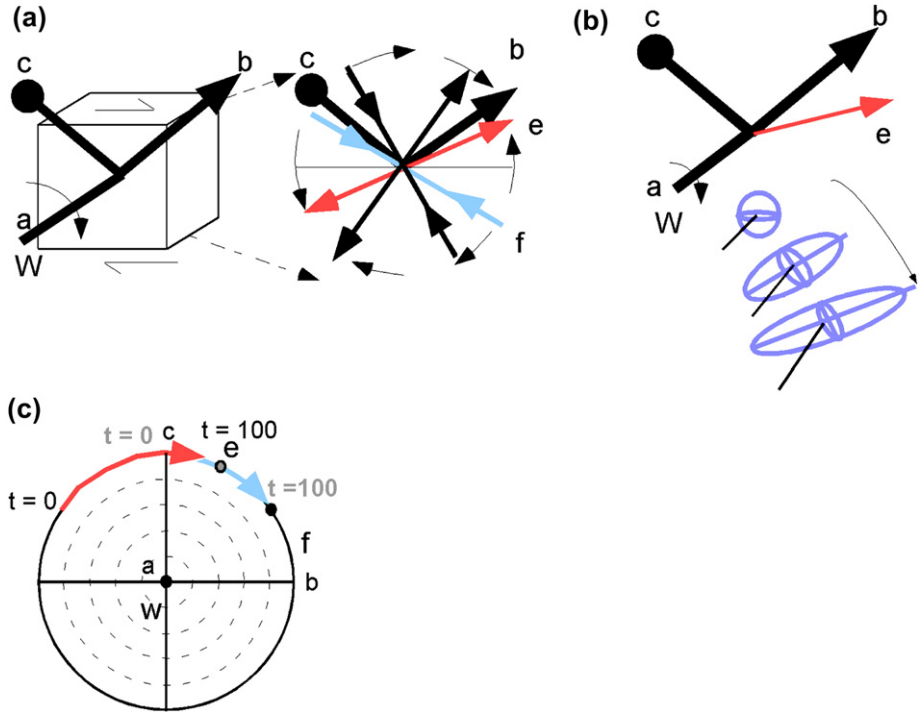

Fig. 1. (a) Schematic representation of the attractor, ISA and material lines geometric relationship within a homogeneous plane strain non-coaxial flow. Thin black line, material lines; Grey lines (e, f), flow eigenvectors of **L**; Bold lines **a**, **b**, **c**, Instantaneous Stretching Axes. (b) Time dependent evolution of the finite strain ellipsoid in a planar non-coaxial flow. Thin line indicates the time dependent evolution from $t = 0$ to $t = 100$ of the main finite strain axes respect to the attractor. Grey line – attractor stable direction (red in the web version); (c) stereographic projection of the time dependent evolution of the finite strain ellipsoid in a monoclinic flow system. Grey arrows, medium finite strain axes path (blue arrows in the web version); Black arrows, principal finite strain axes path (red arrows in the web version); **w**, vorticity vector.

direction on their way from a repulsor to an attractor orientation. A saddle direction exists if the eigenvalues of flow are all different. In any flow type, material lines move towards attractor eigenvectors and this leads to accumulation of foliations and lineations (Passchier, 1997). In this paper we use the term attractor in the most accepted definition: *a set in a phase space (or flow pattern) that has a neighbourhood in which every point remains nearby and approaches the attractor as time goes to infinity* (Conley and Easton, 1971; Ruelle, 1981).

The orientation of flow eigenvectors with respect to ISA does not depend on bulk strain rate or volume change, but exclusively on the rotational properties of the flow. The rotation of all material lines in a flow can balance out, as in pure shear or other coaxial flow types, or have a bulk "residual" rotation component in non-coaxial flow types, such as simple shear. This "residual" component can be expressed by a vorticity vector that describes the size and direction of the residual rotational component of the system with respect to stationary ISA.

1.2. Triclinic flow

In simple non-coaxial flow types, the vorticity vector is parallel to one of the ISA (Fig. 2a, b). This gives the flow pattern a monoclinic shape symmetry, and such flow types are therefore referred to as "monoclinic flow" (Fig. 2c). One of the flow eigenvectors in such systems lies parallel to one of the ISA and the vorticity vector, and the other two in a plane normal to that vector, symmetrically arranged with respect to the remaining ISA. However, in principle there is no reason why the vorticity vector could not have a different direction, oblique to any ISA (Fig. 2d), and such flow types have a triclinic symmetry (Jiang and Williams, 1998). Eigenvectors of triclinic flow are not parallel to the vorticity vector nor to ISA and no eigenvectors are orthogonal. Monoclinic flow can be described by four independent parameters since the possible variations in geometry are small. Triclinic flow, however, needs up to six independent parameters to be defined.

Lin et al. (1998), Jones and Holdsworth (1998) and Jiang and Williams (1998) first drew attention to the possible importance of triclinic flow for geological deformation. Obviously, monoclinic flow with strict symmetry and orthogonal eigenvectors is an idealised model which may not apply to natural flow in inhomogeneous materials. The question is, however, which of the myriad of possible triclinic flow types are relevant for geology. Also, it is not clear if the fabric patterns produced by such triclinic flow will differ much from those produced by monoclinic flow.

For a homogeneous, invariable flow history and after a certain amount of strain accumulation, deformation paths are strictly controlled by flow eigenvectors. In a simple deformation system there is usually a relationship between the orientation of the flow eigenvectors and the finite strain axes (FSA) orientation (Figs. 1b, c and 2a, b). Development of a fabric in a planar deformation zone with rigid wall rocks is well

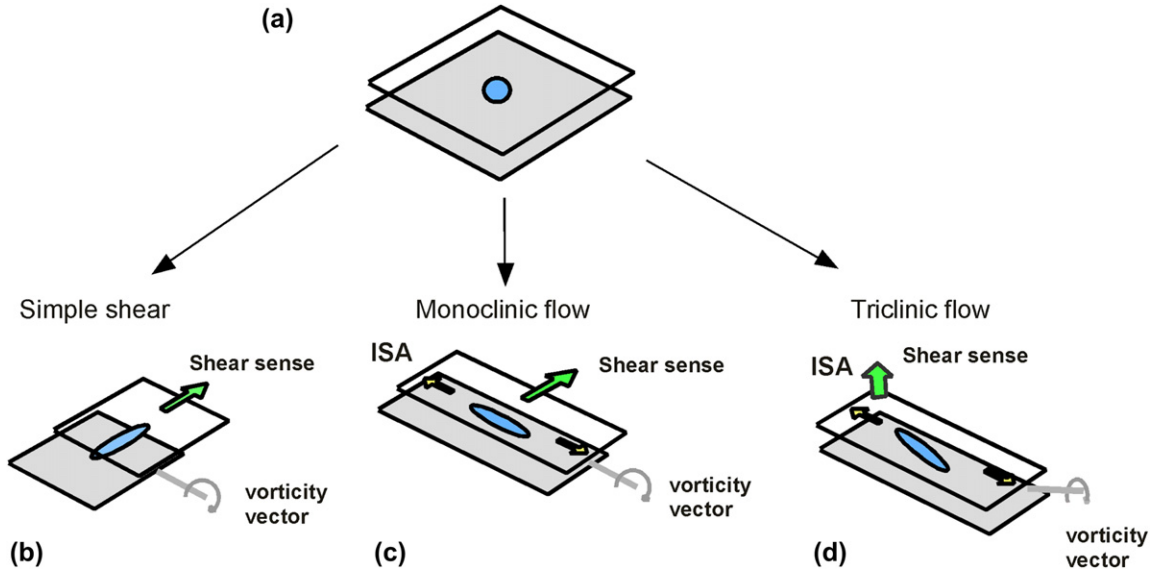

Fig. 2. Sketch of possible shear zone geometries. (a) Undeformed state. (b) Simple shear zone. (c) Monoclinic shear zone: ISA parallel to the vorticity vector. (d) Triclinic shear zone: vorticity vector always obliquely with respect to the ISA. The ellipse shows the orientation of finite strain axes (in the web version: yellow arrows, ISA; green arrows, shear sense; blue ellipses, orientation of finite strain axes).

understood both at the kinematic (Ramsay and Wood, 1973; Ramsay, 1980; Ramsay and Huber, 1983; Gapais et al., 1987; Srivastava et al., 1995) and rheological level (Weijermars, 1991; Regenauer-Lieb and Yuen, 2004 and references therein). In this case, volume constant ductile deformation can only be accommodated by simple shear (Ramsay, 1980; Fig. 1b). This kind of shear zone seems to be common in the upper crust under greenschist to lower amphibolite facies conditions and possibly in the upper mantle, but may be an oversimplification elsewhere. At medium to high grade metamorphic conditions rocks can deform with a progressive deformation history other than simple shear due to deforming wall rocks and volume change. In its simplest form, such progressive deformation operates by monoclinic flow and this simple type of shear zone has been referred to in the literature as a monoclinic shear zone (Simpson and De Paor, 1993; Jiang and White, 1995; Passchier, 1997, 1998), a transpressive shear zone (Harland, 1971; Passchier, 1991; Sanderson, 1976; Kligfield and Crespi, 1984; Sanderson and Marchini, 1984; Krantz, 1995; Jones and Tanner, 1995; Dutton, 1997; Carreras, 2001; Jones et al., 1997, 2004) or stretching and shortening shear zones (Means, 1989; Passchier, 1986). Triclinic shear zones with triclinic flow (Lin et al., 1998; Jiang and Williams, 1998) have been investigated by a number of authors (Carreras and Druguet, 1994; Czeck and Hudleston, 2002; Jones et al., 2004) who described natural examples at meso- and regional scale. Robin and Cruden (1994) have shown numerically that some heterogeneous shear zones can intrinsically have a triclinic flow geometry. These studies, however, used a reference frame linked to eigenvectors in one monoclinic component of general triclinic flow. This means that a change in flow parameters changes the orientation of all triclinic flow axes in an external reference framework. Although results of such studies are completely valid and mathematically correct it is not easy to compare and systematically investigate triclinic flow types using such reference systems. In this paper we have therefore taken another approach. We discuss the characteristics of triclinic flow assuming a homogeneous and steady state flow but using a reference frame in which some initial triclinic flow axes are fixed in the external reference frame even if flow parameters are changed. This makes the comparison between different states of flow easier. The boundary conditions used mean that our flow description can be considered as a linear dynamical system problem. The concept of flow eigenvectors is a property of dynamic systems and is not restricted to a steady state flow system (Ruelle, 1981; Tabor, 1989).

2. Flow kinematics

2.1. Reference frame

In a homogeneously deforming body the rate of displacement of particles in a general reference system x can be described by the Eulerian rate of displacement equation:

$$x_i = \mathbf{L}_{ij} x_j \tag{1}$$

where $\mathbf{L}_{ij}$ is the general tensor of the strain rate defined as:

$$\mathbf{L}_{ij} = \partial v_i / \partial x_j \tag{2}$$

In this study we will discuss steady state flow in which ISA orientation and stretching rates do not change with time (see Means et al., 1980; Passchier, 1997). Obviously such steady state flow will be rare in nature, but the number of possible paths is large and little is presently known of flow paths in progressive deformation. We therefore investigate steady state flow as a reference state for more complex natural systems. This assumption implies that all velocity coefficients are time-independent and that the differential equation in (1) represents a general linear dynamic system where it will be possible to describe and predict

the velocity pattern completely and by integration of (1) also the particle path. The strain rate tensor $\mathbf{L}_{ij}$ can be decomposed into a symmetrical rate of deformation tensor $\mathbf{D}_{ij}$ and an anti-symmetrical vorticity tensor $\mathbf{W}_{ij}$ (Malvern, 1969). These two tensors define the coaxial and the non-coaxial (or rotational) part of a general flow and are defined as:

$$2\mathbf{D}_{ij} = \mathbf{L}_{ij} + \mathbf{L}_{ji} \tag{3}$$

$$2\mathbf{W}_{ij} = \mathbf{L}_{ij} - \mathbf{L}_{ji} \tag{4}$$

Astarita (1979) and Means et al. (1980) have shown that the vorticity tensor in a general reference system can be decomposed as:

$$\mathbf{W}_{ij} = w_{ij} + w'_{ij}, \tag{5}$$

where w_{ij} is the internal vorticity component representing the rotational component of the flow with respect to the ISA, while w'_{ij} represents the spin component of the ISA in the external reference system. This last element is equivalent to a rotation of the deformed body with respect to the external reference system, and therefore cannot influence homogeneous fabric geometry. Only the internal spin component controls the fabric geometry in a homogeneously deforming body (Means et al., 1980). Because of the chosen steady state flow characteristic, the eigenvectors of both $\mathbf{L}_{ij}$ and $\mathbf{D}_{ij}$ matrices represent invariants of the system, are irrotational in the external reference frame and do not change with time. The eigenvectors of the $\mathbf{D}_{ij}$ matrix are the Instantaneous Stretching Axes (ISA) of L and these ISA, **a**, **b** and **c** are orthogonal to each other in steady state flow. ISA are chosen as an internal reference system for any flow type in this paper, where **a**, **b**, **c** coincide with the x, y, z axes of the external reference system. This ISA reference frame is useful since depending on material properties, ISA can be close in orientation to the bulk stress directions for a deformation zone (for an isotropic viscous material example, see Weijermars, 1991; Regenauer-Lieb and Yuen, 2004), or will lie at a fixed angle to the stress axes if the material properties do not change.

2.2. The general triclinic strain rate matrix

In a reference system fixed to the ISA, the general 3D triclinic strain rate matrix can be built in the following way. In a simple monoclinic situation the vorticity vector defined by the tensor $\mathbf{W}_{ij}$ is parallel to one of the ISA. If $\mathbf{L}_{ij} = \mathbf{D}_{ij} + \mathbf{W}_{ij}$, $\boldsymbol{D}_{ij}$ is defined as:

$$\mathbf{D}_{ij} = \begin{pmatrix} \mathbf{a} & 0 & 0 \\ 0 & \mathbf{b} & 0 \\ 0 & 0 & \mathbf{c} \end{pmatrix} \tag{6}$$

and $\mathbf{W}_{ij}$ is defined as:

$$\mathbf{W}_{ij} = \begin{pmatrix} 0 & -w & 0 \\ w & 0 & 0 \\ 0 & 0 & 0 \end{pmatrix} \tag{7}$$

$\mathbf{W}_{ij}$ could also be considered as a vector field curl v, defined as:

$$\mathbf{W}_{ij} = \nabla_{ij} \times v \tag{7a}$$

In this matrix, **a**, **b** and **c** are the stretching rate components (scalar values) of the flow and w is the angular velocity. The vorticity vector $\mathbf{W}_{ij}$ is parallel to **c** (in the initial monoclinic flow) in this description. If we want to "triclinize" the flow we need to rotate the vorticity vector $\mathbf{W}_{ij}$ with respect to **a** and **b** (Fig. 3a) by multiplication of $\mathbf{L}_{ij}$ with one or more rotation matrices. We can combine two rotation operations (as a coordinate transformation) in which the order of composition is not commutative. If we built a new vorticity vector in this way to obtain a general triclinic flow, we need to define three strain rate matrices, which give rise to a rotation by an angle α around **a** in the **bc** plane (**R**(**a**)); by an angle β around **b** (**R**(**b**)) in **ac** plane; and by an angle ϕ around **c** in **ab** plane, respectively (**R**(**c**)), thus:

$$\mathbf{R}(\mathbf{a})_{ij} = \begin{pmatrix} 1 & 0 & 0 \\ 0 & \cos(\alpha) & \sin(\alpha) \\ 0 & -\sin(\alpha) & \cos(\alpha) \end{pmatrix} \tag{8}$$

$$\mathbf{R}(\mathbf{b})_{ij} = \begin{pmatrix} \cos(\beta) & 0 & \sin(\beta) \\ 0 & 1 & 0 \\ -\sin(\beta) & 0 & \cos(\beta) \end{pmatrix} \tag{9}$$

$$\mathbf{R}(\mathbf{c})_{ij} = \begin{pmatrix} \cos(\phi) & \sin(\phi) & 0 \\ -\sin(\phi) & \cos(\phi) & 0 \\ 0 & 0 & 1 \end{pmatrix} \tag{10}$$

In this reference system, we can choose to build the triclinic strain rate matrix in two steps:

A first step consists of rotation of the matrix by angle β or α with respect to the ISA reference frame (Fig. 3a). Since $\mathbf{R}'_{ij} = \mathbf{R}_{ij}^{-1}$, the triclinic strain rate matrices are defined as:

$$\mathbf{L}_{ij} = \mathbf{R}(\mathbf{b})_{ij} \cdot \mathbf{W}_{ij} \cdot \mathbf{R}(\mathbf{b})_{ji} + \mathbf{D}_{ij}$$

or,

$$\mathbf{L}_{ij} = \mathbf{R}(\mathbf{a})_{ij} \cdot \mathbf{W}_{ij} \cdot \mathbf{R}(\mathbf{a})_{ji} + \mathbf{D}_{ij}$$

resulting in:

$$\begin{pmatrix} \mathbf{a} & w(\cos(\beta)) & 0 \\ -w(\cos(\beta)) & \mathbf{b} & w(\sin(\beta)) \\ 0 & -w(\sin(\beta)) & \mathbf{c} \end{pmatrix} \tag{11}$$

or

$$\begin{pmatrix} \mathbf{a} & -w(\sin(\alpha)) & -w(\cos(\alpha)) \\ w(\sin(\alpha)) & \mathbf{b} & 0 \\ w(\cos(\alpha)) & 0 & \mathbf{c} \end{pmatrix} \tag{12}$$

In these matrices, the vorticity vector is obliquely oriented with respect to the ISA but still in one of the ISA planes

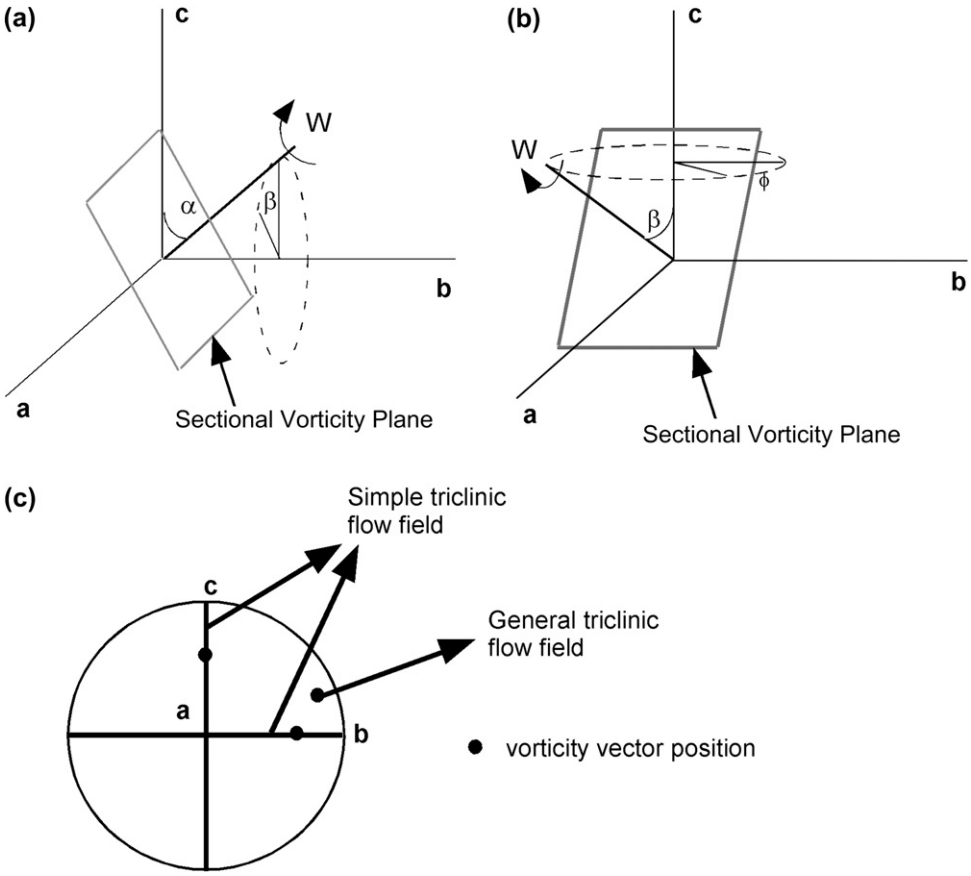

Fig. 3. Reference frame for triclinic flow: **a**, **b**, **c**, Instantaneous Stretching Axes. **w**, vorticity vector. α, β, ϕ, rotation angle of the vorticity vector with respect the ISA. Grey plane represent the sectional vorticity plane. (a) First rotation with respect to **b** (simple triclinic flow) and second rotation with respect to **c** (general triclinic flow). (b) First rotation with respect to **a** (simple triclinic flow) and second rotation with respect to **b** (general triclinic flow). (c) Stereographic ISA-referenced representation of possible vorticity vector positions within simple and general triclinic flow.

(Fig. 3c). We therefore propose to call this flow type **simple triclinic flow**. To obtain the most general triclinic flow tensor we should apply one more rotation (Fig. 3b). Because of the non-commutative property of the matrix product, a unique matrix is not enough to cover the complete spectrum of flow; we need two general strain rate matrices to describe all possible types of triclinic flow. Following the linear transformation law, the rotation of matrix (7) around first **c** and then **a** is defined as:

$$\mathbf{R}(\mathbf{c})_{ij} \times \mathbf{R}(\mathbf{a})_{ij} = \mathbf{U}_{ij}$$

with $\mathbf{L}_{ij} = (\mathbf{U}_{ij} \times \mathbf{W}_{ij} \times \mathbf{U}^{\mathbf{t}}_{\mathbf{ij}}) + \mathbf{D}_{ij}$.

The resulting triclinic strain rate matrix $\mathbf{L}_{ij}$ is:

$$\mathbf{L}_{ij} = \begin{pmatrix} \mathbf{a} & -w\cos(\alpha) & -w\sin(\alpha)\cos(\phi) \\ w\cos(\alpha) & \mathbf{b} & -w\sin(\alpha)\sin(\phi) \\ w\sin(\alpha)\cos(\phi) & w\sin(\alpha)\sin(\phi) & \mathbf{c} \end{pmatrix} \tag{13}$$

The field of possible orientation of the new vorticity vector is in the positive **a**–**b**–**c** quadrants (Fig. 3c). Another possibility to describe general flow (but defining only a half quadrant) could be by rotation first around **b** and then **a** or the inverse rotation composition. In this case the new strain rate tensors are:

$$\mathbf{L}_{ij} = \begin{pmatrix} \mathbf{a} & -w\cos(\alpha)\cos(\beta) & (w\sin(\beta)) \\ w\cos(\alpha)\cos(\beta) & \mathbf{b} & -w\cos(\alpha)\sin(\beta) \\ -w\sin(\beta) & w\cos(\alpha)\sin(\beta) & \mathbf{c} \end{pmatrix} \tag{14}$$

and

$$\mathbf{L}_{ij} = \begin{pmatrix} \mathbf{a} & -w\cos(\beta)\cos(\alpha) & w\cos(\beta)\sin(\alpha) \\ w\cos(\alpha)\cos(\beta) & \mathbf{b} & -w\sin(\beta) \\ -w\cos(\beta)\sin(\alpha) & w\sin(\beta) & \mathbf{c} \end{pmatrix} \tag{15}$$

Strictly speaking only two angles of rotation are necessary to obtain a general triclinic flow, and α, β, or ϕ, are not independent.

In order to compare flow types, it is useful to normalize the magnitude of the vorticity to the stretching rates on the ISA by defining a kinematic vorticity number. Such a number can refer to all three ISA or can be given as a sectional vorticity number that refers only to two ISA (Truesdell, 1954; Ramberg, 1974; Tikoff and Fossen, 1999; Passchier, 1986,

1997; Jiang and Williams, 1998). In a monoclinic flow the maximum sectional vorticity number can be defined simply as:

$$W_n = 2\mathbf{w}/\mathbf{b} - \mathbf{a} \quad (16)$$

where **w** is the magnitude of the vorticity vector that lies parallel to the ISA **c** and **a** and **b** are magnitudes of the two other ISA (Passchier, 1997). This definition can also be used in triclinic flow if the vorticity vector is not parallel to **c** since this does not affect the equation. However, if we keep **w** constant but change the orientation of the vorticity vector, W_n will be identical for different flow types. It is therefore advantageous to use another vorticity number, W_d (d for diagonal) that relates **w** to the projections of the ISA onto a plane normal to the vorticity vector $\mathbf{W}_{ij}$. This diagonal vorticity number defines the maximum vorticity number of the flow. W_d can be defined as (Fig. 3a, b):

$$W_d = 2\mathbf{w}/(\mathbf{b}\cos(\alpha)\cos(\phi) - \mathbf{a}\cos(\beta)) \text{ for(13)} \quad (17)$$

$$W_d = 2\mathbf{w}/(\mathbf{b}\cos(\alpha)\cos(\beta) - \mathbf{a}\cos(\beta)) \text{ for(14)} \quad (18)$$

$$W_d = 2\mathbf{w}/(\mathbf{a}\cos(\alpha)\cos(\beta) - \mathbf{b}\cos(\alpha)) \text{ for(15)} \quad (19)$$

For simple triclinic flow one of the two angles of ''triclinization'' is zero, thereby simplifying the relation. In the case of monoclinic flow (setting α, β, ϕ to zero) W_d coincides with W_n defined by Passchier (1997).

Three other normalised flow parameters have been used to define flow characteristics in monoclinic flow. These are the dilatancy number A_n, the extrusion number T_n and the volume change number V_n. These are not affected by the vorticity and can be defined following Passchier (1997) as:

$$A_n = (\mathbf{a} + \mathbf{b})/(\mathbf{a} - \mathbf{b}) \quad (20a)$$

$$T_n = \mathbf{c}/(\mathbf{a} - \mathbf{b}) \quad (20b)$$

and

$$V_n = (\mathbf{a} + \mathbf{b} + \mathbf{c})/(\mathbf{a} - \mathbf{b}) \quad (21)$$

3. Distribution and field of existence of attractors

3.1. Field of existence of flow eigenvectors

Flow eigenvectors are important since all deformation paths are controlled by them after a certain amount of strain accumulation. It is therefore critical to know how a change in flow parameters changes the orientation of eigenvectors and thus the resulting deformation path. (Ramberg, 1974; Passchier, 1997, 1998). As discussed above, eigenvectors are defined as directions in space in whose orientation material lines and particles are irrotational. Each real eigenvector has an associated real eigenvalue which is a real number that defines the attractor, saddle or repulsor nature of the eigenvector. The most complex flow type is one with three differently oriented eigenvectors with different eigenvalues, as for pure shear flow. However, in the real number domain (or ''field of existence'') the number of eigenvectors can be reduced in two ways; (1) by ''combination'' of two eigenvectors in orientation, as for simple shear with two eigenvectors; or (2) by ''evaporation'' of an eigenvector into what we call a ''ghostvector'' where material lines have minimum or maximum angular velocity but are not irrotational, as for planar rotational flows with $W_d > 1$ (McKenzie, 1979; Weijermars, 1993; Passchier, 1998). Ghostvectors do not have real, but imaginary eigenvalues. In this type of planar flow the ''field of existence'' of the eigenvalues is totally imaginary. Although eigenvectors and ghostvectors may seem to be entirely different entities, they grade into each other by a simple change in the nature of eigenvalues from a real to an imaginary number (Iacopini et al., 2006). Eigenvectors can be recognised in flow patterns since they are apophyses or asymptotes for hyperbolic paths of material line or particle; particles and lines can approach, but not reach the eigenvector. Ghostvectors are crossed by particle paths which are elliptic, spiral or star shaped (Passchier, 1998). In this paper we will demonstrate that within a 3D flow system a clear distinction into strictly real and imaginary domains is not always valid.

In an isochoric monoclinic flow with all kinematic vorticity values W_d between 0 (pure shear) and 1 (simple shear) eigenvalues are real numbers. However, in the case of volume change (or with area increase or decrease in the plane normal to the vorticity vector) eigenvalues can be a mixed combination of real and imaginary numbers in some flow types. As a consequence, the irrotational property of a ''real'' eigenvector changes into a ghostvector where the velocity of a line is maximal or minimal but which cannot permanently attract or repulse it. The important consequence is that no permanent gradually strengthening fabric elements such as foliations or lineations can be built, although pulsating strengthening–weakening fabrics are possible. One of the purposes of this work is to determine under which conditions the number of eigenvectors is reduced by ''combination'' into a single eigenvector or ''evaporation'' into a ghostvector and to establish the extent of the ''field of existence'' of real eigenvalues for different flow parameters in a general triclinic flow.

4. Method

Eigenvalues are defined by the characteristic polynomial of one of the matrices (13)–(15). For a general matrix defining an autonomous flow system in 3D space, the polynomial equation is of the third degree and the roots (i.e. the eigenvalues) are defined by three of the nine solutions typical of a third degree equation. Without going into details of the algebraic procedure used to solve this problem (given in Iacopini, 2005) we will describe the basic analytical constraints (using the flow parameters) that can help to define the real and complex domains of such a flow system. In addition, we use a simple numerical method to find the relation between fields of existence of eigenvalues and flow parameters. All calculations were done using Mathematica 4.1™ (Wolfram Research) and Matlab™ 6.1 (script 1 and 2).

4.1. Analytical method

Consider the general matrix $\mathbf{L}_{ij}$ simplified from Eq. (15):

$$\mathbf{L}_{ij} = \begin{pmatrix} \mathbf{a} & p & -q \\ -p & \mathbf{b} & r \\ q & -r & \mathbf{c} \end{pmatrix} \tag{22}$$

Eigenvalues for a general asymmetrical matrix $\mathbf{L}_{ij}$ of dimension $n = 3$ in C^n space, can be found from the characteristic polynomial:

$$\lambda^3 - \lambda^2(\mathrm{Tr}\,\mathbf{L}_{ij}) + \lambda(p^2 + q^2 + r^2 + \mathbf{ab} + \mathbf{ac} + \mathbf{bc}) - \mathrm{Det}\,\mathbf{L}_{ij} \tag{23a}$$

where λ represents the generic eigenvalues, p, q, r the off-diagonal coefficients of the $\mathbf{L}_{ij}$ strain rate matrix (the angular velocity component of $\mathbf{L}_{ij}$) and **a**, **b**, **c** the diagonal components of the $\mathbf{L}_{ij}$ matrix (the instantaneous stretching rates of $\mathbf{L}_{ij}$). The term Det refers to the determinant of the matrix, while Tr represents the trace of the strain rate matrix. If Eq. (23a) can be solved, the three eigenvalues for the flow are determined and from them the nature of eigenvectors can be found. If an eigenvalue is an imaginary number, no real eigenvector exists for that eigenvalue, only a ''ghostvector''. Eq. (23a) can be solved as follows.

The algebraic substitutions:

$$u = p^2 + q^2 + r^2 + \mathbf{ab} + \mathbf{ac} + \mathbf{bc} \tag{23b}$$

$$v = (\mathrm{Tr}\,\mathbf{L}_{ij}) \tag{23c}$$

$$k = -\mathrm{Det}\,\mathbf{L}_{ij} \tag{23d}$$

simplify Eq. (23a) to:

$$\lambda^3 - \lambda^2 v + \lambda u + k \tag{23e}$$

Using the further substitutions:

$$\lambda = y - v/3 \tag{23f}$$

$$j = u - v^2/3 \tag{23g}$$

$$h = k + (uv)/3 - 2v^3/27 \tag{23h}$$

Eq. (23e) is modified to:

$$y^3 + yj + h \tag{24}$$

Third order polynomials of this type can be solved if we put $y = m + n$, implying from Eq. (23f) that $\lambda = m + n - v/3$. Substituting we obtain:

$$\begin{aligned} y^3 + yj + h &= (m+n)^3 + j(m+n) + h \\ &= m^3 + 3m^2 n + 3n^3 n + n^3 + j(m+n) + h \\ &= (m^3 + n^3 + h) + (m+n)(3mn + j) \end{aligned} \tag{25}$$

Eq. (25) is equivalent to the simplified Eq. (24) and the general solutions of this new third degree equation are defined by the following boundary conditions:

$$-h = m^3 + n^3 \tag{26a}$$

and

$$nm = -j/3 \tag{26b}$$

Before solving these two equations and in order to simplify the solution procedure it is necessary to introduce a useful property: it is demonstrated that if m and n are solutions in a general second degree equation, the correspondent second degree equation has the form:

$$Z^2 - (m+n)z + mn \tag{26c}$$

If we rewrite solution (26a) by cubing (26b) we have:

$$-h = m^3 + n^3 \tag{27a}$$

$$m^3 n^3 = -j^3/27. \tag{27b}$$

Now Eqs. (27a) and (27b) have the same form as the roots of the second degree system (26c) so that as consequence Eq. (24) is equivalent to:

$$Z^2 + hZ - j^3/27 = 0 \tag{28}$$

Solving Eq. (28) and using the substitution in (23b)–(23d) it follows that:

$$m = \left(-h/2 - \left(h^2/4 + j^3/27\right)^{1/2} \right)^{1/3} \tag{29a}$$

$$n = \left(-h/2 + \left(h^2/4 + j^3/27\right)^{1/2} \right)^{1/3} \tag{29b}$$

Because of the applied cubing (27b), m and n have to satisfy the relation $mn = -j/3$ and the solutions are of the type:

$$\lambda_i = m + n - v/3. \tag{30}$$

In order to have an idea of the field of existence of real eigenvalues as a function of the velocity **w** and the stretching rate **a**, **b**, **c**, we have to study the solution defined by Eqs. (23a), (24) and (28) after inserting all substitutions made in Eqs. (23b)–(23h).

In the initial strain rate matrices, Eqs. (13), (14) and (15), the strain rate and velocity components have real values so that all coefficients in our solution in Eq. (30) are real. The sets of boundary conditions expressed in Eqs. (28) and (29) define nine possible solutions, only three of which will satisfy both the third degree equation and the boundary conditions stated in Eqs. (26) and (27).

This relation in its extended form is complicated but their solutions depend mainly on the quadratic roots of relations (29a) and (29b) defined by:

$$\Delta = \left(h^2/4 + j^3/27\right) \tag{31}$$

We can have the following three situations: $\Delta > 0$, $\Delta = 0$ or $\Delta < 0$.

Below, we will consider each of these situations in turn.

1) $\Delta > 0$

If $\Delta > 0$, $h^2/4 > -j^3/27$ and the three solutions (and the eigenvalues of the dynamical system) are two complex numbers and one real number, inducing an evaporation of two eigenvectors. Unlike the two dimensional situation (Ramberg, 1974; McKenzie, 1979; Weijermars, 1993), eigenvalue fields of existence completely controlled by imaginary eigenvalues cannot exist in 3D. The real number is the eigenvalue,

$$\lambda_1 = m + n - \left(\left(\mathrm{Tr}\,\mathbf{L}_{ij}\right)/3\right)$$

and the other two are,

$$\lambda_2 = m\left(\frac{-1+i\sqrt{3}}{2}\right) + n\left(\frac{-1-i\sqrt{3}}{2}\right) - \frac{\mathrm{Tr}\,\mathbf{L}_{ij}}{3} \tag{32a}$$

and,

$$\lambda_3 = m\left(\frac{-1-i\sqrt{3}}{2}\right) + n\left(\frac{-1+i\sqrt{3}}{2}\right) - \frac{\mathrm{Tr}\,\mathbf{L}_{ij}}{3} \tag{32b}$$

The main problem is to determine which eigenvalue controls the accumulation of the fabric at large strain (for $t \to \infty$). In our 3D case for stable fabric development, the real eigenvalue has to be the one dominating for $t \to \infty$, implying a long time of strain accumulation. If complex eigenvalues dominate, they will influence the fabric development producing pulsating and closed deformation paths (complete treatment in Iacopini, 2005). Therefore, the following statements are valid if we observe the deformation path in the plane normal to the vorticity vector:

If $\lambda_1 = 0$, particles move in planes, and two situations are possible. If λ_2 and λ_3 are purely imaginary the flow pattern is a set of embedded ellipses giving rise to a pulsating pattern (Ramberg, 1974; Weijermars, 1993). If λ_2 and λ_3 also have a real part then, depending on their sign, particles move in a stable or a non-stable spiral.

If λ_1 is positive (or negative) we have a 3D flow path and there can be, three situations:

a) If λ_2 and λ_3 are purely imaginary we have a pulsating strain with a repelling (or attracting) component parallel to the vorticity vector (Fig. 4a).
b) If λ_2 and λ_3 have a real component that is negative, particles tend to migrate inwards in a stable spiral to an equilibrium point which is reached after a large amount of strain with a repulsing (or attracting) component parallel to the vorticity vector (Fig. 4b).
c) If λ_2 and λ_3 have a real part that is positive, points tend to migrate outwards in a non-stable spiral towards or away from an attractor (or repulsor) axis in the third dimension (Fig. 4c).

In all cases the real eigenvalue has no pulsating "history" and could induce development of a stable fabric.

2) $\Delta = 0$

If $\Delta = 0$ then according to Eqs. (29), (30) and (31):

$$n = m = (-h/2)^{1/3} \tag{33}$$

and the three eigenvalues are all real numbers as follows:

$$\lambda_1 = 2(-h/2)^{1/3} + \mathrm{Tr}\,\mathbf{L}_{ij}/3 \tag{34a}$$

$$\lambda_2 = 2\cos(2\pi/3)(-h/2)^{1/3} = -(-h/2)^{1/3} + \mathrm{Tr}\,\mathbf{L}_{ij}/3 \tag{34b}$$

$$\lambda_3 = 2\cos(4\pi/3)(-h/2)^{1/3} = -(-h/2)^{1/3} + \mathrm{Tr}\,\mathbf{L}_{ij}/3 \tag{34c}$$

This implies that we have three solutions, but two of them are coincident inducing a combination of two eigenvectors. If the two eigenvalues $\lambda_2 = \lambda_3$ are negative, we have a deformation path known as a stable improper node as shown in Fig. 4d (with a third component parallel to the vorticity axes). If $\lambda_2 = \lambda_3$ are positive we have a stable improper node as shown in Fig. 4e. $\lambda_2 = \lambda_3 = 0$ represents simple shear (with $\epsilon_i = 0$) as described by Ramberg (1974) and shown in Fig. 4f.

3) $\Delta < 0$

In this case m and n are two complex conjugate numbers following the boundary condition given in Eq. (19). This implies that if $\Delta < 0$ the solutions for λ are all real number solutions (products or sums of conjugate imaginary number are always real). The relations are:

$$\lambda_1 = 2\,\mathrm{Cos}(\delta)(-p/3)^{1/2} + \mathrm{Tr}\,\mathbf{L}_{ij}/3 \tag{35a}$$

$$\lambda_2 = (-p/3)^{1/2}(\mathrm{Cos}(\delta + 2\pi)/3) + \mathrm{Tr}\,\mathbf{L}_{ij}/3 \tag{35b}$$

$$\lambda_3 = (-p/3)(\mathrm{Cos}(\delta + 2\pi)/3) + \mathrm{Tr}\,\mathbf{L}_{ij}/3 \tag{35c}$$

with

$$\mathrm{Tan}(\delta) = -\left((-R)^{1/2}\right)q/2 \tag{36}$$

Examples are given in Table 1a–c. W_n^* is the threshold non-normalised vorticity number, W_d is the diagonal vorticity number (following relations (17)–(19)) and W_d^* is the threshold maximum vorticity number above which the eigenvalue starts to be imaginary.

In the case of $\Delta < 0$, $W_d < W_d^*$ so that all eigenvalues are permanently positive and define real eigenvectors.

The following types of eigenvalue distributions are possible:

For $\lambda_1 > 0 > \lambda_2 > \lambda_3$ a flow pattern (or deformation paths) of saddle axes is defined, with one attractor corresponding to the negative eigenvalue and a repulsor associated with the larger eigenvalue (Fig. 5a).

$\lambda_1 > \lambda_2 > 0 > \lambda_3$ defines a situation of non-volume constant flow extruding in one direction.

If $\lambda_1 = 0$, $0 > \lambda_2 > \lambda_3$ there is a stable attractor (all particles attracted to the stable eigenvector, Fig. 5b) and if $\lambda_1 > \lambda_2 > 0$, $\lambda_3 = 0$ and $\lambda_1 > \lambda_2 > \lambda_3 > 0$ non-stable expanding flow patterns will develop (Fig. 5c).

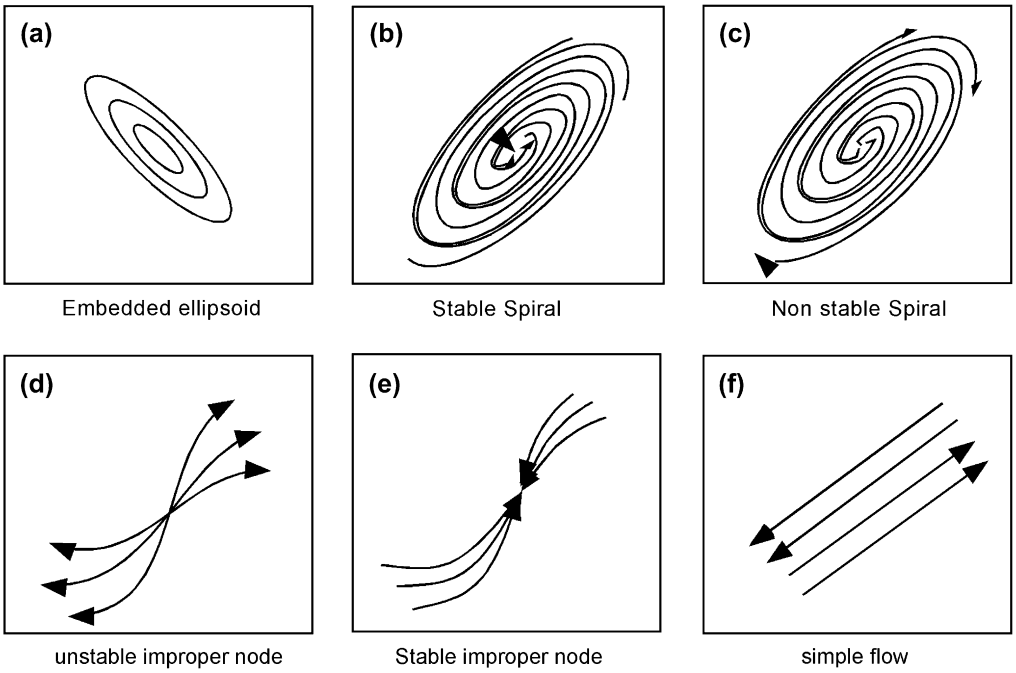

Fig. 4. Schematic representation of some principal flow patterns as seen in the sectional vorticity plane. (a) Closed elliptical pattern; (b) stable spiral; (c) unstable spiral; (d) unstable improper node pattern; (e) stable improper node pattern; (f) simple flow pattern. Small arrow, flow direction.

5. Triclinic flow and real eigenvector distributions

For simple triclinic flow types with volume change the field of existence of real eigenvalues depends on the angle of triclinization. Tables 1a–c shows limiting values W_d^* for some simple triclinic flow examples within the range of possible deviation of the vorticity vector with respect to one of the ISA. Fig. 6 shows the limiting value W_d^* for all possible volume constant and non-constant simple triclinic flows within a deviation of 0.4 radians. As a general trend it is clear that both for constant volume (Table 1a, Fig. 6) and in the case of volume change (Tables 1b, c; Fig. 6) an increased ''triclinization'' of the flow leads to a smaller real field of existence of eigenvalues for high vorticity numbers of the flow (compare a and d in Fig. 6 for each W_d^* value). In volume constant triclinic flow a deviation of 0.3 radians of the vorticity vector from one of the ISA gives a limiting vorticity number of 0.82. A complete trend of critical vorticity values within a simple triclinic flow for $0 < A_n < 1$ and $0 < T_n < 1$ is shown in Fig. 6. These values show that:

a) as general trend with increasing triclinization (α varying from 0.1 to 0.4) the field of existence of real eigenvalues tends to become smaller (Fig. 6a to d). At a high vorticity number the triclinic geometry is controlled by two imaginary eigenvalues;
b) with increasing dilatancy of flow ($A_n > 0$ and $T_n = 0$), implying a volume increase, the critical value W_d^* tends to restrain the ''real'' field of existence of triclinic flow (Fig. 6);
c) with increasing extrusion number T_n in the absence of dilatation, the field of existence of imaginary flow tends to disappear and real triclinic flow exists up to high vorticity values (Fig. 6); and

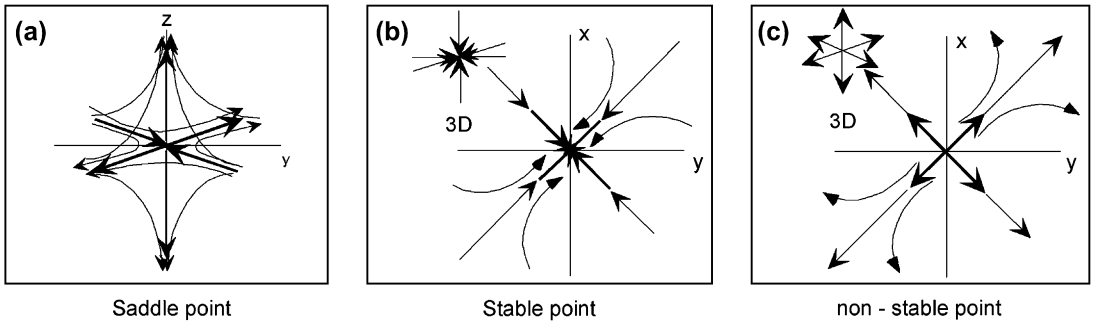

Fig. 5. Possible 3D flow patterns for real eigenvalue fields of existence. Views are parallel to the vorticity vector. *x,y*, general reference frame (close to ISA in triclinic flow). Bold lines, principal eigenvectors. Thin lines approximate flow paths in the neighbourhood of the eigenvectors. Flow types can have a saddle point (a), a stable point (b) or a non-stable point (c).

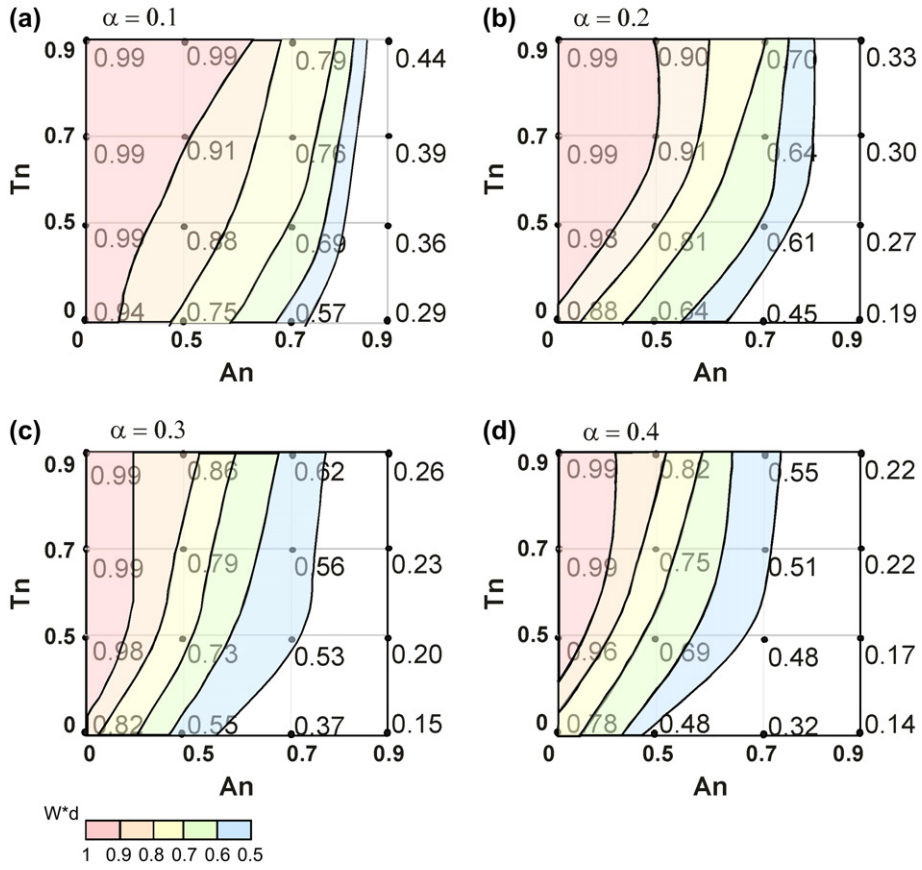

Fig. 6. Graph showing contours for the threshold W_d^* vorticity number at which imaginary eigenvalues appear at different flow parameters. (a) $\alpha = 0.1$ radians; (b) $\alpha = 0.2$ radians; (c) $\alpha = 0.3$ radians; (d) $\alpha = 0.4$ radians. Points in the diagrams correspond to exact calculated values of vorticity numbers W_d^* at different flow parameters. A_n, dilatancy number; T_n, extrusion number. α, angle of rotation of the vorticity vector. Grey scale bar-field of existence of different vorticity threshold values W_d^*. Colour scale bar-field of existence of different vorticity threshold values W_d^* in web.

d) if we mix the effects of the two flow parameters A_n and T_n, the field of existence tends to be small with respect to the volume constant example (Fig. 6).

In order to provide a visualisation of what happens to eigenvectors when flow deviates from monoclinic, i.e. when the vorticity vector moves away from one of the ISA, a Matlab code (ScienceDirect script 1) was used to calculate eigenvector positions. We plotted the path traced by the eigenvector for different flow parameters in stereograms (Figs. 7–10). This was done for simple and general triclinic flow types in the real domain range. Fig. 7 shows the distribution of the three

Table 1a
Threshold vorticity numbers defining the imaginary eigenvalue fields of existence in the case of constant volume ($\mathbf{a} = -\mathbf{b}$, $\lambda_1 > 0 > \lambda_2 > \lambda_3$)

α or β	$\mathbf{w}^*$	W_n^*	W_d^*
0.1	0.47	0.96	0.94
0.2	0.44	0.88	0.88
0.3	0.41	0.83	0.82
0.4	0.39	0.81	0.78
0.5	0.36	0.76	0.72
0.6	0.34	0.74	0.68
0.7	0.32	0.72	0.64
0.8	0.30	0.70	0.60
0.9	0.29	0.70	0.58
1.0	0.27	0.71	0.54
1.1	0.26	0.76	0.52
1.2	0.25	0.78	0.50
1.3	0.25	0.86	0.50

W, angular velocity; W_n, monoclinic vorticity number sensu Passchier (1998); W_d^*, maximum vorticity number for a triclinic flow system. α and β represent rotation angles of the vorticity vector (see text).

Table 1b
Threshold vorticity numbers defining the imaginary eigenvalue fields of existence in the case of volume change ($\mathbf{a} = 0.7$, $\mathbf{b} = -0.5$; $\lambda_1 > \lambda_2 > 0 > \lambda_3$)

β	$\mathbf{w}^*$	W_n^*	W_d^*
0.1	0.58	0.96	0.96
0.2	0.56	0.93	0.94
0.3	0.53	0.88	0.90
0.4	0.50	0.83	0.86
0.5	0.48	0.80	0.84
0.6	0.45	0.75	0.80
0.7	0.43	0.73	0.79
0.8	0.41	0.68	0.78
0.9	0.39	0.65	0.77
1.0	0.38	0.63	0.79
1.1	0.37	0.61	0.81
1.2	0.36	0.60	0.83
1.3	0.35	0.58	0.89

Variables same as that of Table 1a.

Table 1c
Threshold vorticity numbers defining the imaginary eigenvalue fields of existence in the case of volume change ($\mathbf{a} = 0.7$, $\mathbf{b} = -0.5$; $\lambda_1 > 0 > \lambda_2 > \lambda_3$

α	**w***	W_n^*	W_d^*
0.1	0.58	0.90	0.90
0.2	0.56	0.83	0.84
0.3	0.53	0.70	0.78
0.4	0.50	0.63	0.73
0.5	0.48	0.58	0.68
0.6	0.45	0.55	0.64
0.7	0.43	0.51	0.63
0.8	0.41	0.48	0.62
0.9	0.39	0.46	0.62
1.0	0.38	0.45	0.63
1.1	0.37	0.43	0.66
1.2	0.36	0.41	0.69
1.3	0.35	0.40	0.74

Variables same as that of Table 1a. α represent rotation angle of the vorticity vector.

eigenvectors for a constant volume simple triclinic flow at three fixed angles of triclinization (0.1, 0.2, 0.3 radians). Boldness of the curve for each eigenvector indicates the magnitude of the corresponding eigenvalue. In all examples the orientation of the eigenvectors changes from a monoclinic basis situation for fixed flow parameters towards an angle of ''triclinization'' that limits the field of real eigenvector behaviour. In most examples the three eigenvalues are all real with two negative and one positive value so that the flow pattern has a saddle shape (as in Fig. 5a). Some interesting conclusions can be drawn from the examples (Figs 7a–c, 8a–f): a small deviation of the vorticity vector from parallelism to one of the ISA induces a non-symmetrical distribution of all eigenvectors with respect to the ISA. As soon as the flow is ''triclinized'', eigenvectors gradually move away from the planes of the ISA. If W_d is changed at a fixed angle of ''triclinization'' until the eigenvalues assume real values (0–0.8), the possible deviation of the principal eigenvectors from a monoclinic pattern is below 0.2 radians (see Fig. 7a–c). If for a specific W_d the orientation of the vorticity vector is changed, the final obliquity and the trace-length of eigenvector curves are strongly dependent on the components of the vorticity (Fig. 8). In domains with low kinematic vorticity numbers (Fig. 8a–c), the field of existence of real eigenvalues is larger than in domain with high vorticity numbers (Fig. 8d–f). In both cases the maximum positive eigenvalues (for $\alpha = 0$, Fig. 8a) and/or minimum negative eigenvalues (for $\beta = 0$, Fig. 8b) that control the flow pattern for $t \to \infty$, show a small deviation from the ISA of less then 0.3 radians. For high vorticity numbers ($\sim$0.8) the eigenvalues have a limited field of existence (Fig. 8d–f) and the extensional stable eigenvectors (Fig. 8d, e) show a limited possible deviation from the ISA of between the 0.2 and 0.4 radians. Eigenvectors associated with the lowest eigenvalues show the same attitude. Only the medium eigenvalues which are relatively unimportant in controlling the flow pattern show a strong variability (Fig. 8d–f). If we extend the analysis to non-constant volume at different extrusion (T_n) or dilatancy numbers (A_n) this phenomenon is confirmed at both high (Fig. 9) and low vorticity numbers (Fig. 10). Figs. 9 and 10 clearly show that the deviation of the maximum eigenvector from an ISA position exceeds 0.3 radians only for very high T_n values (Fig. 9c, e and Fig. 10g, l) and generally the maximum eigenvector develops along the extrusion direction. For dilatant flow without (Fig. 10b, c) and with extrusion (Fig. 9d, f and Fig. 10d, e, f, h, i, m, n) or at plane strain (Figs. 8a, 9a and 10a), the maximum and minimum eigenvectors are not easily recognizable since they deviate less than 0.1 radians from the ISA. The observations described above indicate that the distribution of eigenvectors in simple triclinic flow cannot strongly deviate from a monoclinic symmetry, even if they are oblique to ISA and have a complicated geometry. It is also shown that the field of existence is strongly controlled by the kinematic vorticity number. These observations, however, apply to simple triclinic flow. In the case of general triclinic flow the eigenvectors show a significantly deviating distribution under some circumstances (Fig. 8c, f). However, even in these cases, eigenvalues adopt imaginary values at high vorticity numbers (Table 1a–c).

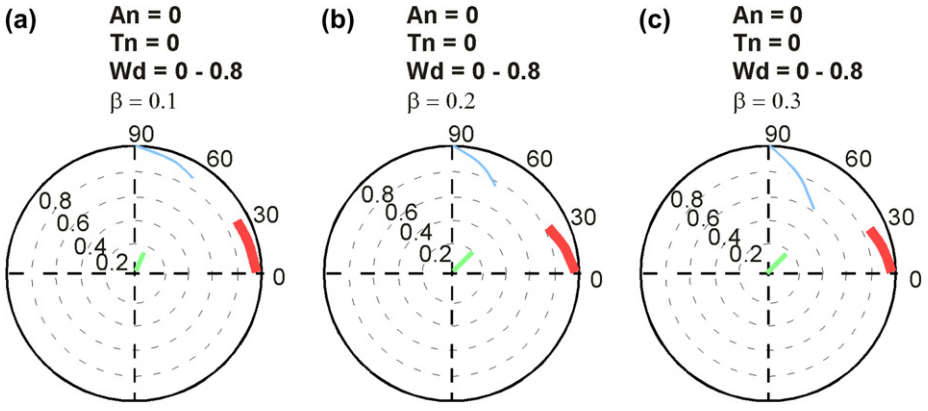

Fig. 7. Change in flow eigenvector orientation as a function of a change in vorticity number (up to $W_d < 0.8$) for three simple triclinic flow types (a–c). The three curves show the path of the eigenvectors. β represent rotation angle of the vorticity vector around b. Line thickness refers to the magnitude of the eigenvalues. The deviation of the three eigenvectors with respect to monoclinic geometry cannot exceed 0.2 radians. Further discussion in text (Line colors in the web version refer to the magnitude of the eigenvalues. Red, maximum eigenvalues; green, medium eigenvalue; blue, minimum eigenvalue).

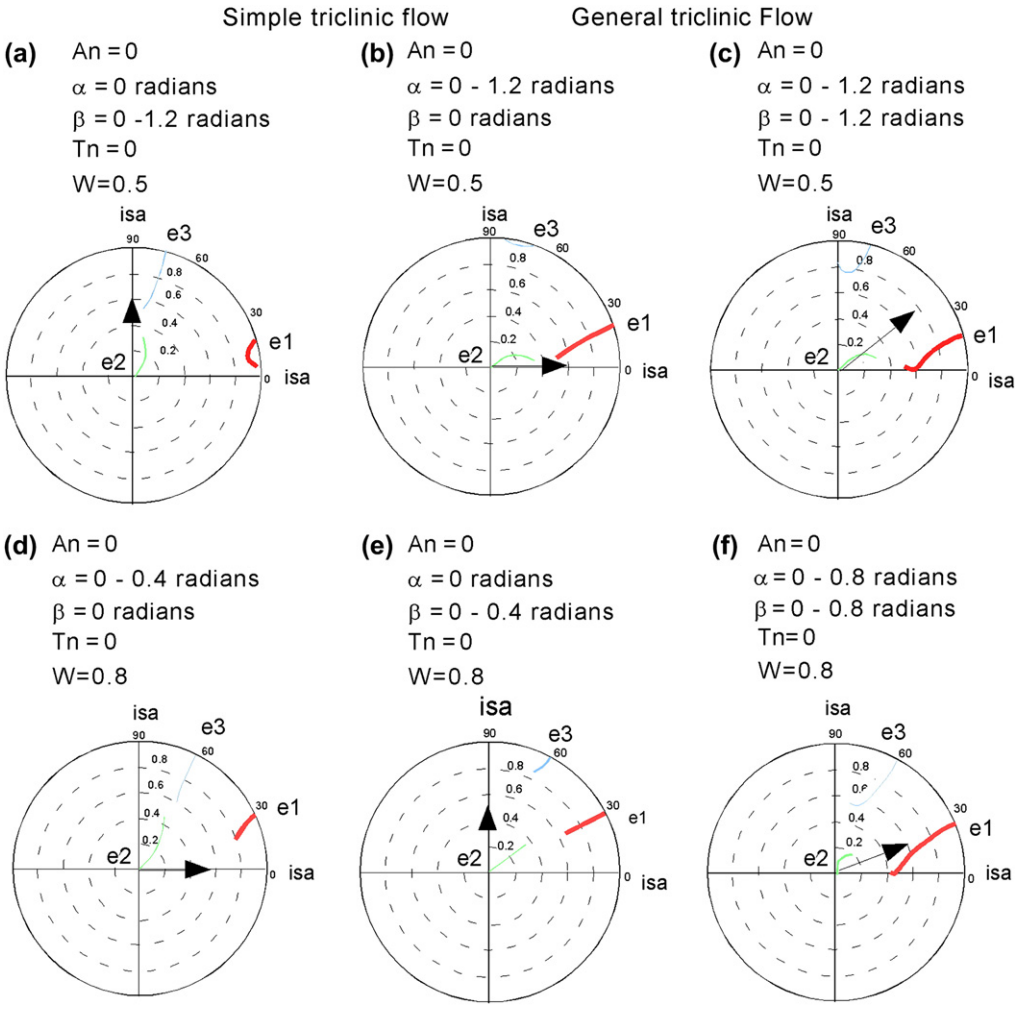

Fig. 8. Change in flow eigenvector orientation as a function of change in orientation of the vorticity vector in an ISA reference system. Line thickness refers to the magnitude of the eigenvalues (Line colors in the web version refer to the magnitude of the eigenvalues. α and β represent rotation angles of the vorticity vector (see text). Red, maximum eigenvalues; green, medium eigenvalue; blue, minimum eigenvalue). (a)–(c) Vorticity number $W_d = 0.5$. (d)–(f) Vorticity number $W_d = 0.8$. The maximum finite strain axis will tend to accumulate (for $t \rightarrow \infty$) at the thickest curve, which is the position of the attractor eigenvector.

6. Numerical approach

Although it is useful to know the position of eigenvectors in a flow type, it is difficult to understand their meaning in terms of flow patterns and progressive deformation, since it is not clear how material lines rotate in space. A more intuitive and practical way to understand the rotation of material lines (even if less exact) is to reproduce the flow pattern by calculating the displacement of particles with progressive deformation. We calculated such displacement patterns for simple triclinic flow using a Matlab code (ScienceDirect script 2). In this simple simulation we assume an initial random distribution of material points (defined by a Monte Carlo distribution) which are displaced by a deformation matrix. The deformation matrix in this case is the first derivative of the strain rate matrix as a first approximation of the deformation path. The code links the position of each point to its position in the next time step in order to recognize a first order flow pattern, but also to define the distribution of the principal attractor directions. To obtain a clear pattern with a clear distribution of attractor directions it is enough to reapply the strain matrix to the population of particles 4–5 times. As the number of possible flow geometries is limitless we have chosen some simple but supposedly realistic situations assuming both area and volume change for different vorticity numbers between 0 and 1 and with different angular orientation of the vorticity vector. Real eigenvector deformation paths are plotted showing the attractor and repulsor axes for different flow parameters. They represent the flow pattern of our dynamical system for the different flow parameters. The limit of such a method is that imaginary eigenvectors cannot be represented by the program code.

In the first two rows of Fig. 11 some end-member monoclinic flow types are shown with different flow parameters. These patterns are identical to those presented by Passchier (1997) and we can use them as a basis for the interpretation of relative weak triclinic patterns shown in the next two rows.

Flow in Fig. 11a, b, e and f, shows a flow pattern around a saddle point in which one eigenvector (with the largest eigenvalue) defines a repulsor from which points migrate

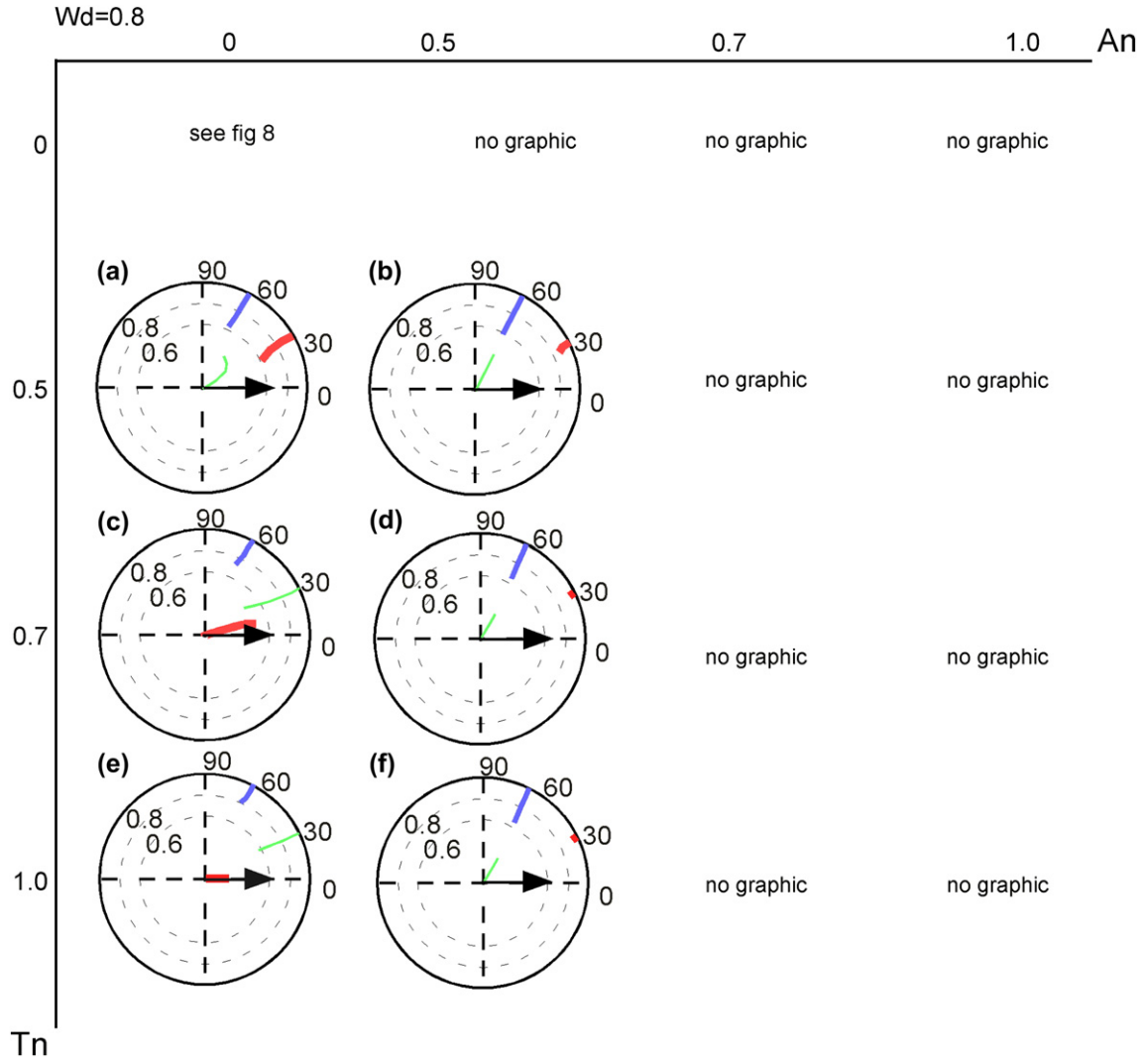

Fig. 9. Change in flow eigenvector orientation as a function of change in orientation of the vorticity vector around a, in an ISA reference system for different flow parameters in a simple triclinic flow (Line colors in the web version refer to the magnitude of the eigenvalues. Red, maximum eigenvalues; green, medium eigenvalue; blue, minimum eigenvalue). Line thickness refers to the magnitude of the eigenvalues. Vorticity number $W_d = 0.8$. α, Angle of rotation of the vorticity vector around x. The maximum finite strain axis will tend to accumulate (for $t \rightarrow \infty$) at the thickest curve, which is the position of the attractor eigenvector. The black arrows indicate the direction of movement of the vorticity vector at different angles of triclinization.

away; whereas the eigenvector defined by the smallest negative eigenvalue is the attractor toward which points tend to migrate. The third eigenvector, which can be positive or negative depending on whether there is extrusion or not along the **c** axis is normal to the other two in a stereogram. If we triclinize the flow (Fig. 11c, d, g, h) the flow pattern still contains a saddle axis but now the directions of the extruding attractors are obliquely disposed and no longer parallel to ISA. The intermediate eigenvector also moves away from the vertical giving rise to movement within the **bc** plane. Fig. 11i and l show monoclinic examples with a flow pattern around a non-stable axis. Flow is dilatant ($A_n = 1.5$) with two different vorticity values. The dilatancy implies positive eigenvalues and the two eigenvectors are both unstable. Triclinization of this flow (Fig. 11m, n) results in an asymmetric pattern defined by three positive eigenvalues with a still recognizable principal direction (Fig. 11m, n). The last two flow patterns (Fig. 11o, p) represent flow types that are ‘‘simple shear controlled’’ flow with a high vorticity number. The two eigenvalues tend to assume similar values, with the same positive (Fig. 11o) or negative (Fig. 11p) sign. This last flow pattern is characterised by negative dilatancy ($A_n \leq 0$), with a stable positive eigenvector along which the points tend to accumulate. As shown earlier, there are no real flow patterns with real eigenvectors for corresponding triclinic flow but the pattern is expected to behave as a stable spiral (Iacopini et al., 2006). The modelling presented in Fig. 11 shows that attractor eigenvectors derived from the simulations do not deviate much from those calculated analytically. This suggests that even though this method is inaccurate and produces patterns that are not identical to those described by an exact progressive matrix, they are a good first approximation of the progressive deformation matrix (see also Tikoff and Fossen, 1993).

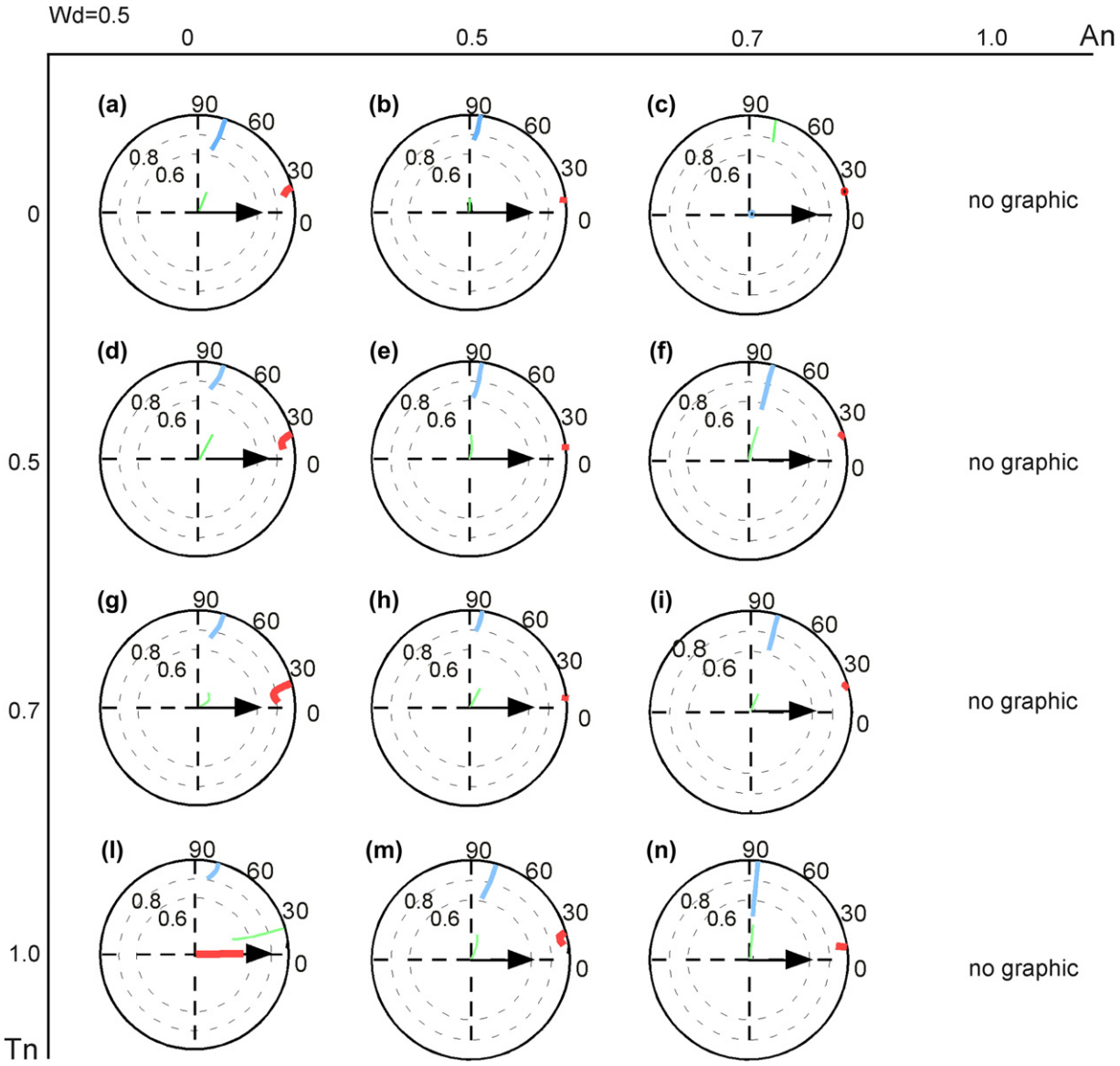

Fig. 10. Change in flow eigenvector orientation as a function of change in orientation of the vorticity vector around a, in an ISA reference system for different flow parameters in a simple triclinic flow (Line colors in the web version refer to the magnitude of the eigenvalues. Red, maximum eigenvalues; green, medium eigenvalue; blue, minimum eigenvalue). Line thickness refers to the magnitude of the eigenvalues. Vorticity number $W_d = 0.5$. Vorticity vector is rotated around a, assuming different α values till the eigenvalues assume real number values. The maximum finite strain axis will tend to accumulate (for $t \rightarrow \infty$) at the thickest curve, which is the position of the attractor eigenvector. Where eigenvalues become imaginary, no diagram is shown. The black arrows indicate the direction of movement of the vorticity vector at different angles of triclinization.

7. Progressive strain matrix, finite ellipsoid and their geological meaning

So far we limited our analytical approach to the spatial distribution of the principal attractors and their change in orientation and properties with changing flow parameters, including the rotation of material lines and/or the motion of single particles in flow and progressive deformation. This is useful but insufficient to understand fabric accumulation in rocks. For that purpose it is necessary to know how finite strain accumulates with progressive deformation. For this reason we calculated the developing strain ellipsoid in progressive deformation and its relation with the eigenvectors for triclinic flow. In order to derive the time dependent progressive strain matrix we solved the differential equation according to the classical method following Fossen and Tikoff (1993), Soto (1997), and Jiang and Williams (1998). Because of the asymmetry and complete initial form of the strain rate matrix defined in Eqs. (13), (14) and (15), the result is a rather complex matrix, a function of angles, angular velocity and strain elements. If the strain matrix is defined by $\mathbf{F}_{ij}$, then the finite ellipsoid matrix is defined by the Cauchy–Euler tensor $\mathbf{F}^{*}_{ij} \times \mathbf{F}^{t}_{ij}$. The eigenvectors of this ellipsoid define the finite strain axes (FSA). Examples of the distribution of finite strain ellipsoid principal axes in a shear zone with triclinic flow were presented by Robin and Cruden (1994), Jiang and Williams (1998), Czeck and

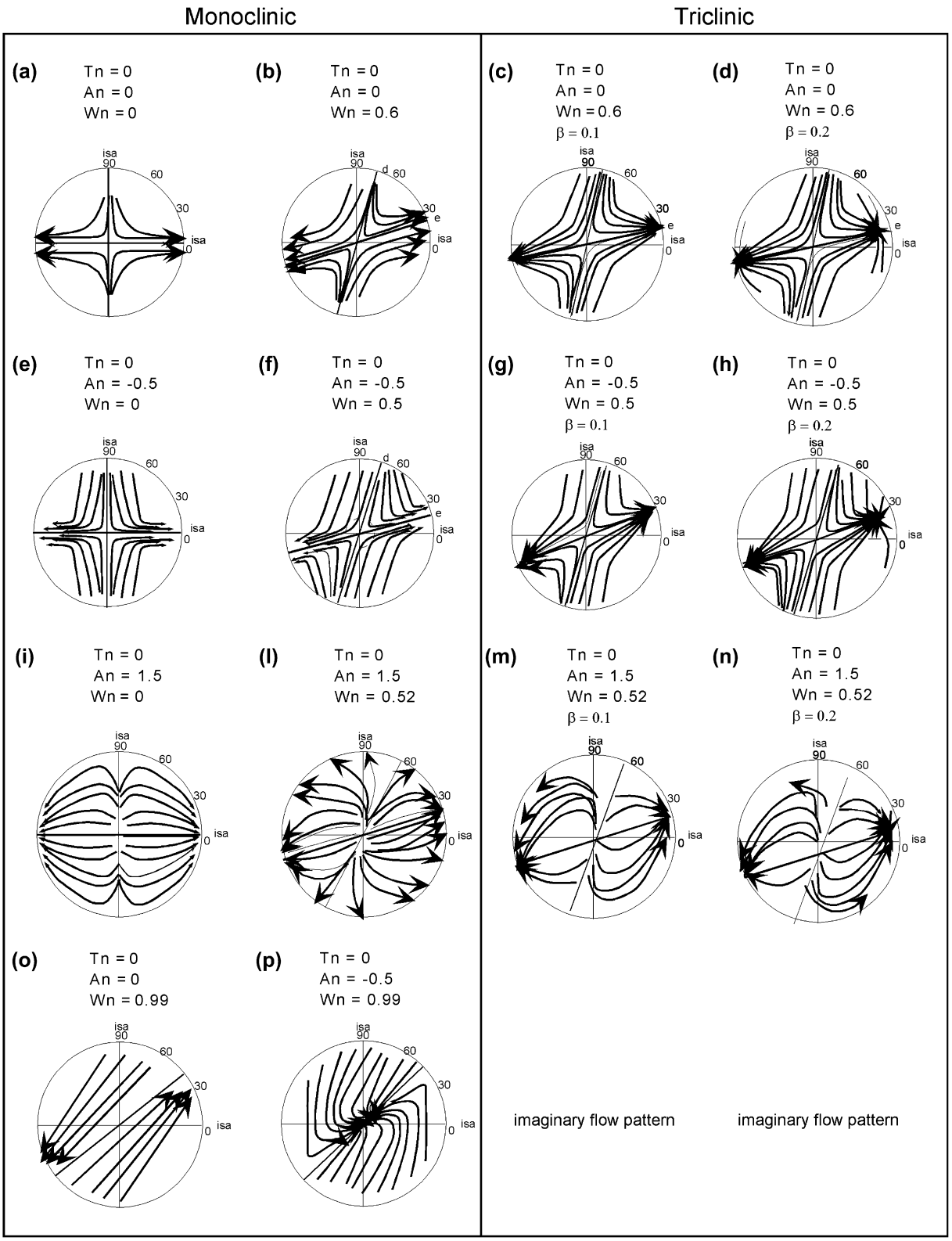

Fig. 11. Flow patterns for different monoclinic and triclinic flow parameters.

Hudleston (2002) and Jones et al. (2004). These authors have choose an external reference frame that was fixed with respect to the shear zone boundaries and considered to be in a stable position throughout the evolution of the system. This configuration is useful to describe a pattern with respect to physical boundaries but the assumption does not mathematically represent a rigorous fixed reference system (Passchier, 1986). In order to avoid this assumption we choose to plot

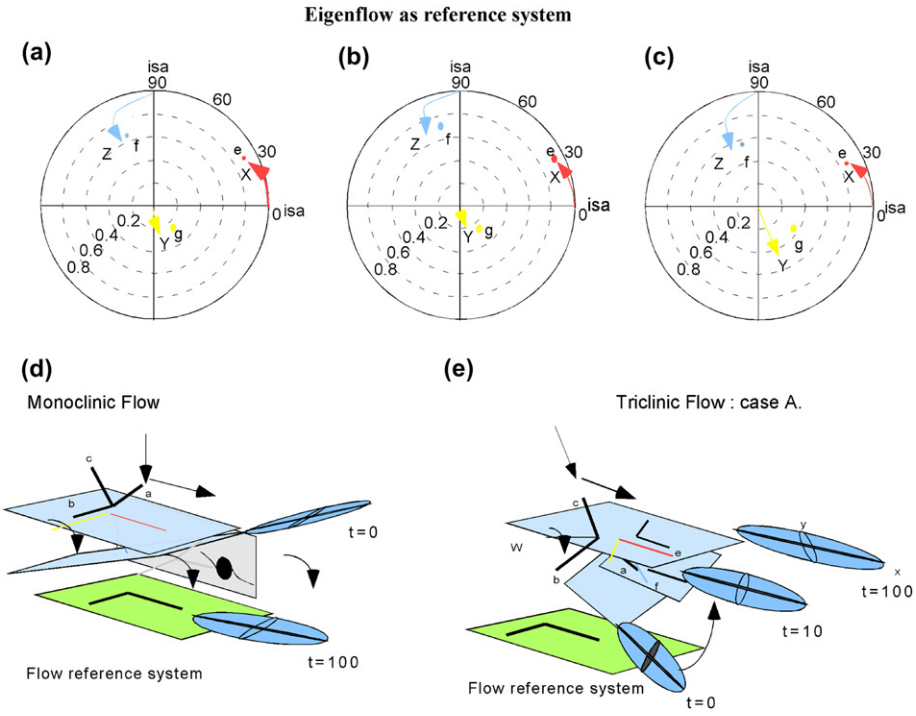

Fig. 12. (a)–(c) Path of the principal finite strain axes with progressive deformation at $W_d^* = 0.6$. (a) $\beta = 0.1$. (b) $\beta = 0.2$. (c) $\beta = 0.3$. (d) Sketch of the finite strain ellipsoid orientation in monoclinic flow at time $t = 0$ to $t = 100$ in a flow eigenvector reference system. (e) Sketch of the finite strain ellipsoid orientation in triclinic flow as in (a) at time $t = 0$ to $t = 100$ in a flow eigenvector reference system. Red line – main fabric attractor; yellow line – medium eigenvector; **a, b, c** – ISA in web.

the finite strain axes with respect to the flow eigenvectors or ISA and to present some simple examples for both situations. Obviously, this complicates visualisation considerably since shear zone boundaries in the system can deform in the chosen reference frame. It is clear, however, that this setting gives rise to finite strain axes patterns that are different from those shown by the authors mentioned above. Nevertheless the two approaches are physically equivalent. Fig. 12 shows migration of finite strain axes in a simple triclinic shear zone where the vorticity vector lies in the **bc** ISA plane at 0.1, 0.2 or 0.3 radians (Fig. 12a–c) from the mean axis **b** as shown in Fig. 12d. This is the same initial flow condition as shown in Fig. 11c, d and very similar to the monoclinic flow condition shown in Figs. 11b and 12c. The direction of motion of the finite strain axes are shown by arrows in the stereograms and their position for three different triclinic situations at $t = 0$,10, 20, 30, 40, 50 are given in Table 2a, b, c. Fig. 12e represents the situation shown in the stereogram in Fig. 12a at $t = 0$, 10 and 100. At $t = 0$ the principal finite strain axis starts from the ISA direction and move with progressive deformation towards the principal extensional eigenvector. The other two strain axes rotate as well, with the intermediate strain axis plunging in the same direction as the second eigenvector, but never coinciding since flow eigenvectors are not orthogonal in this case. It can be demonstrated (Iacopini, 2005) that the principal strain axis (X) is always controlled by the principal attractor and this implies that the XY finite strain plane, if it exists, will tend to rotate toward the principal eigenflow plane (see also Hobbs et al., 1982). This gives rise to an oblique distribution of the finite strain axes with respect to the ISA (Fig. 12e).

8. Discussion

8.1. Potential application

In the previous sections we have shown how the pattern of flow eigenvectors and notably the attractors in the real number domain control both the distribution of material lines and finite strain axes in a general flow system. In a homogeneous continuum, strain axes can define a linear and planar shape fabric. This has been shown both analytically (Ramberg, 1974; Soto, 1997; Passchier, 1998; Iacopini, 2005) and experimentally for analogue materials (Piazolo et al., 2000). Such fabric growth with progressive deformation is not obvious when two eigenvectors are imaginary since the flow pattern will cause pulsating strengthening–weakening fabric development that will hamper or inhibit the development of a stable fabric.

If the assumption of constant flow parameters is relaxed and flow parameters can change in the course of time, albeit in constant volume deformation, ‘‘linear attractors’’ could still be defined during the progressive deformation history (Tabor, 1989). In this case the mathematical considerations developed above would still predict the fabric distribution. In the case of in homogeneous flow the kinematic frame becomes more complicated. If we adapt a model in which the strain is defined by a continuous gradient (Fig. 13a; Ingles, 1983; Robin and Cruden, 1994; Jones et al., 2004) the following statements can be made:

a) some authors (Treagus and Lisle, 1997) demonstrated that in steady state 2D and 3D situations that are controlled by

Table 2
Finite strain axis orientation in an ISA reference frame, labelled in radians, at $t = 0$, 10, 20, 30, 40, 50

Shear example a	Shear example b	Shear example c
0.99999, 0.00196, 0.00000; 0.00000, −0.0003, 1.00000; −0.00196, 0.9999, 0.00039;	0.99998; 0.01910; 0.00000; 0.00000; −0.00591; 1.00000; 0.00191; −0.99999; −0.00059;	0.99998; 0.00198; 0.0000; 0.00000; −0.00198; 1.0000; −0.00198; 0.99998; 0.0000;
0.99980; 0.0195; −0.00007; 0.00000, −0.0039, −0.99992; −0.01958, 0.9998, −0.00397;	0.99982; 0.01861; 0.00010; 0.00000; −0.00576; 0.99998; 0.01861; −0.99981; −0.00576;	0.99980; 0.01988; 0.0000; 0.00000; −0.00199; 0.9999; −0.01988; 0.99980; 0.0001;
0.98357; 0.1803; −0.00711; 0.00000; −0.0394; 0.99922; −0.18049; 0.9828; 0.03876;	0.98517; 0.17128; 0.00975; 0.00000; −0.05706; 0.99837; 0.17156; −0.98356; −0.05622;	0.98306; 0.18322; 0.0003; 0.00000; −0.01981; 0.9998; −0.18325; 0.98287; 0.0194;
0.90974; 0.4095; 0.06824; 0.00093; −0.1663; 0.98605; −0.41517; 0.8969; 0.15176;	0.92033; 0.38065; 0.08996; 0.00250; −0.23574; 0.97181; 0.39113; −0.89416; −0.21795;	0.90620; 0.42134; 0.0355; 0.00012; −0.08430; 0.9964; −0.42284; 0.90272; 0.0764;
0.90032; 0.4221; 0.10600; 0.03110; −0.3055; 0.95168; −0.43411; 0.8535; 0.28818;	0.91325; 0.38610; 0.12993; 0.17271; −0.65582; 0.73488; 0.36896; −0.64870; −0.66562;	0.89642; 0.4400; 0.0526; 0.00071; −0.1201; 0.9927; −0.44319; 0.8898; 0.1079;
0.90032; 0.4422; 0.10608; −0.41883; 0.9065; 0.05244; 0.0027; −0.1183; 0.99297	0.91324; 0.38610; 0.12993; 0.40432; −0.89807; 0.17313; 0.04988; −0.21065; −0.97628;	0.89591; 0.4404; 0.0577; 0.00127; −0.1326; 0.9911; −0.44422; 0.8879; 0.1194

heterogeneous deformation, principal stress and strain surfaces do not necessarily exist, and this possibly also applies to incremental strain in homogeneous 3D flow; and

b) on the other hand a "pseudo-plane" (sensu Treagus and Lisle, 1997) and lineation exist in such cases and this "pseudo-plane" does not change orientation in a randomly way but is controlled by a stable direction in steady state deformation such as that of an attractor (Treagus and Lisle, 1997). Therefore, the finite strain ellipsoid will move towards the "local" attractor directions, the orientation of

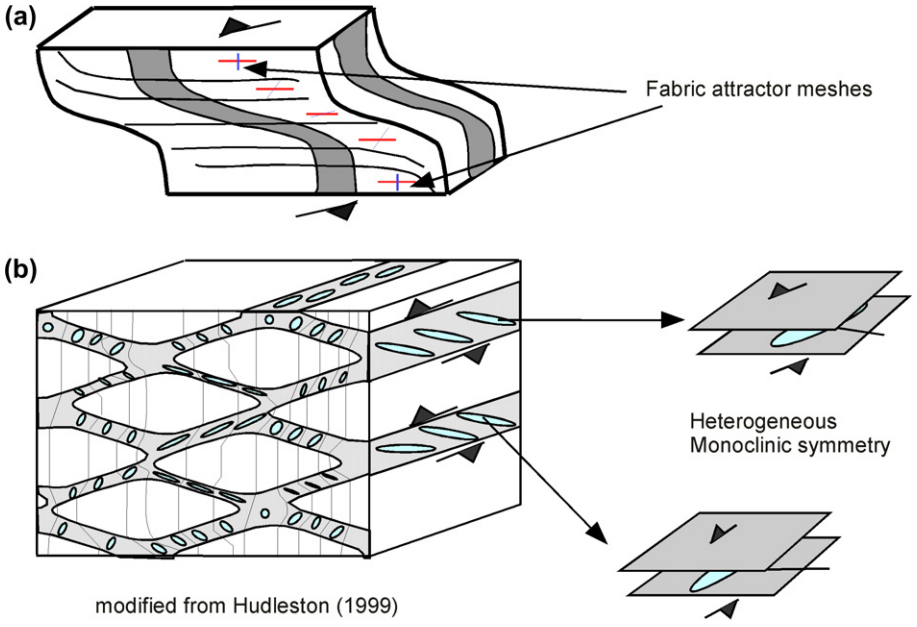

Fig. 13. (a) Example of a heterogeneous shear zone defined by a continuous strain gradient. The shear zones can be characterised by the trend of attractors defining an attractor mesh. If the gradient can be defined as a continuous function the distribution of the main flow eigenvector can be predicted (in the web version: red lines, main attractors; blue lines, main repulsors). (b) Example of a shear zone network surrounding domains of low strain (in the web version: blue ellipses, finite strain ellipsoids). Black arrows, shear sense movement.

which may vary laterally. In this heterogeneous context, following Passchier (1997), it is more realistic to speak of attractor meshes (Fig. 13a). This means that finite strain axes can define a lineation and foliation plane (provided they exist, Treagus and Lisle, 1997) at high strain in all types of steady state flow. If so the following conclusions can be drawn from our modelling work:

(1) In Figs. 7 (a–c), 8 (a–f), 9 (a–f) and 10 (a–f) bold curves indicate the orientation of the principal stretching attractor eigenvector with respect to the ISA. For high strain accumulation this attractor will be the line towards which the *X*-axis of finite strain, and therefore the stretching lineation, will converge. We have seen in the simple triclinic flow examples given above that the stretching lineation has a space variability and deviation from the ISA plane ranging between 0 and 0.4 radians. This means that it can deviate over a range of 20° from ISA orientations, and this is the true deviation from the initial monoclinic situation in any reference system. In order to define the *XY* plane of finite strain (if it exists), it is necessary to see how both eigenvectors that can act as attractors are oriented. It was shown above that the *Y* finite strain axis has a plunge that is similar to the direction of the second eigenvector. The orientation of the *XY* plane is therefore controlled between the ISA and the flow eigenvector system has a similar orientation range as the lineation. For non-extruding systems in shear zones with a high vorticity number, a small deviation from monoclinic flow (less than 10°) produces stretching lineations and foliation planes that also deviate less than 10° from a monoclinic geometry (Fig. 7). For shear zones with a significant pure shear component (low vorticity number) the fabric can deviate up to 20° from monoclinic symmetry. Similar results for low angles of triclinization were obtained, in a different reference system, by Jiang and Williams (1997 – in their paper defined as $\phi \leq 20°$ and high Θ).
(2) In high strain shear zones (with high vorticity numbers) simple triclinic flow can be expected only if the system is strongly extruding along a principal direction.
(3) In isotropic rocks, ISA can be close in orientation to principal stress axes (Weijermars, 1991; Regenauer-Lieb and Yuen, 2004). In this case, the orientation of the vorticity vector is strongly controlled by the intermediate stress axis (parallel to one of the ISA).

This implies that the flow geometry in a homogeneous medium will be monoclinic (Passchier, 1997) or a ''weak'' simple triclinic flow. This suggests that even if general triclinic flow could theoretically develop, triclinic fabric geometry should be very rare in high strain shear zones that are strongly controlled by the stress field. We think that high strain zones which operated by high vorticity numbers in isotropic medium are most likely dominated by monoclinic flow or simple triclinic flow with a symmetry that is close to monoclinic. To better constrain such considerations, the effect of applied stress on the flow symmetry distribution within real high strain shear zones should be further investigated (Fletcher and Pollard, 1999).

8.2. Limits of the homogeneous model

Although homogeneous flow is a simple and useful mathematical assumption, flow in most natural situations is not only inhomogeneous but also strongly partitioned. In fact several field examples suggest that ductile shear zones nucleate on or directly overprint previous anisotropies (e.g. an existing foliation, Carreras, 2001). Alternatively, ductile shear zones may overprint a brittle fracture system, evolving to a network of widening coalesced mylonitic shear zones (Passchier, 1984; Mancktelow and Pennacchioni, 2005; Fusseis et al., 2006). In both cases shear zones represent localisation of strain where a homogeneous model cannot be applied for the entire deformation history. In these settings the analytical prediction of a mesoscopic fabric is complicated since the strain rate matrix is both time and space dependent. However, the following qualitative considerations can help to suggest possible scenarios:

(1) After a large amount of strain accumulation, a dense network of mylonitic shear zones could form, separating low strain domains (Fig. 13b). In this case the assumption of continuous flow and a steady state deformation history does not apply and this limits the application of the kinematic model proposed. Each shear zone segment in the network may be characterised by different strain accumulation and may have a different orientation of the vorticity vector (inset in Fig. 13b), leading to a different local fabric. The result will be a complex fabric geometry, even if flow in individual shear zone segments was monoclinic. In this setting the effect of heterogeneity could be far more important then a flow symmetry effect such as triclinic versus monoclinic flow. Supposed triclinic shear zones should be analysed for this effect.
(2) Likely places where triclinic flow may be important are anisotropic rocks and/or high grade deformed rocks oblique to the stress field, in March-fixed or March rotating rocks with medium-low vorticity component (sensu March, 1932; Tikoff and Teyssier, 1994). Another possibility is magma flow between deformable wall rocks (assuming a Jeffery Model; Tikoff and Teyssier, 1994; Czeck and Hudleston, 2002) inducing a strong extruding component. Detailed analysis of the fabric distribution in such extruding systems could help to test and unravel possible triclinic models.

9. Conclusions

(1) Flow eigenvectors can act as attractors of material points and lines in monoclinic and triclinic flow types. Such attractors can also act as barriers for finite strain axes. As

a consequence linear and planar shape fabrics tend to rotate toward the attractor eigenvector orientation in space.

(2) Flow eigenvectors and thus attractors, only act as barriers if corresponding eigenvalues are real. In 3D, even the imaginary field always has one real eigenvalue and depending on its relative dominance it could cause deviation of the shape fabric geometry from well-known 2D patterns.

(3) For many triclinic flow types, especially at high vorticity number (as in high strain shear zones) eigenvalues are imaginary numbers. This implies that no stable deformation fabric can accumulate in such flow types. Triclinic flow with developing shape fabrics can only exist if ''triclinicity'' is limited, e.g. if the angle between the vorticity vector and ISA is small or if the system is extruding. This is particularly valid at high vorticity numbers.

(4) Realistic fabric forming triclinic flow patterns within volume constant deformation can only form fabrics that lie up to 20° from the orientation expected from monoclinic flow. It is questionable if such triclinic flow histories can be recognised in nature.

Acknowledgements

R.Toussaint is thanked for his patience in the improvement of the analytical part of this paper. M Barsanti, E. Iacopini, G. Molli, C. Montomoli, P.C. Pertusati, S. Seno, E. Tavarnelli and B. Tikoff are thanked for their helpful comments and encouragement. The extended stay of D.I in Mainz would have been impossible without the extra-funds from the Doctorate School of the University of Pisa. The Dipartimento di Matematica Applicata of University of Pisa is thanked for providing Matlab during the work in Pisa. Richard Jones and Haakon Fossen are thanked for their illuminating and constructive reviewing. R. Holdsworth is thanked for kind editorial work.

Appendix A. Supplementary information

Supplementary data associated with this article can be found, in the online version, at doi:10.1016/j.jsg.2006.10.002.

References

Astarita, G., 1979. Objective and generally applicable criteria for flow classification. Journal of Non-Newtonian Fluid Mechanics 6, 69–76.

Bobyarchick, A.R., 1986. The eigenvalues of steady state flow in Mohr space. Tectonophysics 122, 35–51.

Carreras, J., 2001. Zooming on the Northern Cap de Creus shear zones. Journal of Structural Geology 23, 1457–1486.

Carreras, J., Druguet, E., 1994. Structural zonation as a result of inhomogeneous non coaxial deformation and its control on syntectonic intrusions: an example from the Cap de Creus area, eastern Pyrenees. Journal of Structural Geology 16, 1525–1534.

Conley, R., Easton, R., 1971. Isolate invariant set and isolated blocks. Transactions of the American Mathematical Society 158, 35–61.

Czeck, M.D., Hudleston, P.J., 2002. Testing models for obliquely plunging lineations in transpression. A natural example and theoretical discussion. Journal of Structural Geology 25, 959–982.

Dutton, B.J., 1997. Finite strain in transpression zones with no boundary slip. Journal of Structural Geology 19, 1189–1200.

Fletcher, R.C., Pollard, D.D., 1999. Can we understand structural and tectonic processes and their products without appeal to a complete mechanics? Journal of Structural Geology 21, 1071–1088.

Fossen, H., Tikoff, B., 1993. The deformation matrix for simultaneous pure shear, simple shear and volume change and its application to transtension and transpression tectonics. Journal of Structural Geology 15, 413–422.

Fusseis, F., Handy, M.R., Schrank, C., 2006. Networking of shear zones at the brittle to viscous transition (Cap de Creus, NE Spain). Journal of Structural Geology 28, 1228–1443.

Gapais, D., Balé, P., Choukroune, P., Cobbold, P.R., Mahjoub, Y., Marquer, D., 1987. Bulk kinematics from shear zone patterns: some field examples. Journal of Structural Geology 9, 635–646.

Harland, W.B., 1971. Tectonic transpression in Caledonian Spitzbergen. Geological Magazine 108, 27–42.

Hobbs, B.E., Means, W.D., Williams, P.F., 1982. The relationship between foliation and strain: an experimental investigation. Journal of Structural Geology 4, 411–428.

Iacopini, D., 2005. Kinematics of General Flow Systems, from Shear Zones to Transpressive System: A Numerical and Analytical Approach and a Field Example from the Sardinian Variscan Belts. PhD thesis, University of Pisa.

Iacopini, D., Passchier, C.W., Koehn, D., Carosi, R., 2006. Complex eigenflows in 3D flow system. Geophysical Research Abstract, EGU 2006-Vienna 8, 08353.

Ingles, J., 1983. Theoretical strain patterns in ductile zones simultaneously undergoing simple and bulk shortening. Journal of Structural Geology 5, 369–382.

Jiang, D., White, J.C., 1995. Kinematics of rock flow and the interpretation of geological structures, with particular reference to shear zones. Journal of Structural Geology 17, 1249–1265.

Jiang, D., Williams, P.F., 1998. High strain zone: a unified model. Journal of Structural Geology 20, 1105–1120.

Jones, R.R., Holdsworth, R.E., 1998. Oblique simple shear in transpression zones. In: Holdsworth, R.E., Strachan, R.A., Dewey, J.F. (Eds.), Continental Transpressional and Transtensional Tectonics. Geological Society, London, Special Publications, vol. 135, pp. 35–41.

Jones, R.R., Holdsworth, R.E., Bailey, W., 1997. Lateral extrusion in transpression zones: the importance of boundary conditions. Journal of Structural Geology 19, 1201–1217.

Jones, R.R., Tanner, P.W.G., 1995. Strain partitioning in transpression zones. Journal of Structural Geology 17, 793–802.

Jones, R.R., Holdsworth, R.E., Clegg, O., McCaffrey, K.J.W., Tavarnelli, E., 2004. Inclined transpression. Journal of Structural Geology 26, 1531–1548.

Kligfield, R., Crespi, J., 1984. Displacement and strain pattern of extensional orogens. Tectonics 3, 577–609.

Krantz, R.W., 1995. The transpressional strain model applied to strike slip, oblique convergent and oblique-divergent deformation. Journal of Structural Geology 17, 1125–1137.

Lin, S., Jiang, D., Williams, P.F., 1998. Transpression (or transtension) zones of triclinic symmetry: natural example and theoretical modelling. In: Holdsworth, R.E., Strachan, R.A., Dewey, J.F. (Eds.), Continental Transpressional and Transtensional Tectonics. Geological Society, London, Special Publications, vol. 135, pp. 41–57.

Malvern, L., 1969. Introduction to the Mechanic of a Continuous Medium. Prenctice-Hall, Englewood Cliffs, New Jersey.

Mancktelow, N.L., Pennacchioni, G., 2005. The control of precursor brittle fracture and fluid–rock interaction on the development of single and paired shear zones. Journal of Structural Geology 27, 645–661.

March, A., 1932. Mathematische Theorie der Regelung nach der Korngestalt bei affiner Deformation. Zeitkrift fur Kristallografie 81, 285–297.

McKenzie, D., 1979. Finite deformation during fluid flow. Geophysical Journal of Royal Astronomical Society 58, 689–715.

Means, W.D., 1989. Stretching faults. Geology 17, 893–896.

Means, W.D., Hobbs, B.E., Lister, G.S., Williams, P.F., 1980. Vorticity and non-coaxiality in progressive deformations. Journal of Structural Geology 2, 371–378.

Passchier, C.W., 1984. The generation of ductile and brittle shear bands in a low angle mylonite zone. Journal of Structural Geology 6, 273–281.
Passchier, C.W., 1986. Flow in natural shear zone-the consequence of spinning flow regimes. Earth Planetary Sciences Letters 77, 70–80.
Passchier, C.W., 1991. Analysis of deformation paths in shear zones. Geologische Rundschau 77, 308–318.
Passchier, C.W., 1997. The fabric attractor. Journal of Structural Geology 19, 113–127.
Passchier, C.W., 1998. Monoclinic model shear zones. Journal of Structural Geology 20, 1121–1137.
Piazolo, S., ten Grotenhuis, S., Passchier, C.W., 2000. New apparatus for controlled general flow modeling of analog material. In: Koyi, H.A., Mancktelow, N.S. (Eds.), Tectonic Modeling. A Volume in Honor of Hans Ramberg: Boulder Colorado. Geological Society of America Memoir, vol. 193, pp. 235–244.
Ramberg, H., 1974. Particle paths, displacement and progressive strain applicable to rocks. Tectonophysics 28, 1–37.
Ramsay, J.G., 1980. Shear zones geometry: a review. Journal of Structural. Geology 2, 83–89.
Ramsay, J.G., Graham, R.H., 1970. Strain variation in shear belts. Canadian Journal of Earth Sciences 7, 786–813.
Ramsay, J.G., Huber, M.I., 1983. The Techniques of Modern Structural Geology, vol. 1. Academic Press.
Ramsay, J.G., Wood, D.S., 1973. The geometric effect of volume change during deformation processes. Tectonophysics 16, 263–277.
Regenauer-Lieb, K., Yuen, D.A., 2004. Positive feedback of interacting ductile fault from coupling equation of state, rheology and thermal – mechanics. Physics of the Earth and Planetary Interiors 142, 113–135.
Robin, P.Y., Cruden, A.R., 1994. Strain and vorticity pattern in ideally ductile transpression zones. Journal of Structural Geology 16, 447–466.
Ruelle, D., 1981. Small random perturbations of dynamical systems and the definition of attractors. Communication of Mathematical Physics 82, 137–151.
Sanderson, D.J., 1976. The superposition of compaction and plane strain. Tectonophysics 30, 35–54.
Sanderson, D.J., Marchini, A., 1984. Transpression. Journal of Structural Geology 6, 449–549.
Simpson, C., De Paor, D., 1993. Strain and kinematic analysis in general shear zones. Journal of Structural Geology 15, 1–20.
Soto, A., 1997. A general deformation matrix for three dimension. Mathematical Geology 29, 93–130.
Srivastava, D.C., Hudleston, P.J., Earley III, D., 1995. Strain and possible volume loss in high grade ductile shear zone. Journal of Structural Geology 17, 1217–1231.
Tabor, M., 1989. Chaos and Integratibility in Non-linear Dynamics: An Introduction. Wiley & Sons., New York.
Tikoff, H., Fossen, B., 1993. Simultaneous pure and simple shear: the unifying deformation matrix. Tectonophysics 217, 267–283.
Tikoff, B., Fossen, H., 1999. Three dimensional reference deformations and strain facies. Journal of Structural Geology 21, 1497–1512.
Tikoff, B., Teyssier, C., 1994. Strain and fabric analysis based on porphyroclast interaction. Journal of Structural Geology 16, 24–35.
Treagus, S., Lisle, R., 1997. Do principal surfaces of stress and strain always exist? Journal of Structural Geology 19, 997–1010.
Truesdell, C., 1954. The Kinematic of Vorticity. Indiana University Press, Bloomington.
Weijermars, R., 1991. The role of stress in ductile deformation. Journal Structural Geology 13, 1061–1078.
Weijermars, R., 1993. Pulsating strain. Tectonophysics 220, 51–67.